UNIVERSITY OF BIRMINGHAM
University of Birmingham Research at Birmingham

Local buckling behaviour of high-strength steel tubular columns subjected to one-sided cyclic loading and implications in seismic design of steel MRFs

Hamauzu, Shingo; Skalomenos, Konstantinos; Kurata, Masahiro ; Theofanous, Marios

DOI:
10.1016/j.soildyn.2021.107115

License:
Creative Commons: Attribution-NonCommercial-NoDerivs (CC BY-NC-ND)

Document Version
Peer reviewed version

Citation for published version (Harvard):
Hamauzu, S, Skalomenos, K, Kurata, M & Theofanous, M 2022, 'Local buckling behaviour of high-strength steel tubular columns subjected to one-sided cyclic loading and implications in seismic design of steel MRFs', *Soil Dynamics and Earthquake Engineering*, vol. 154, 107115. https://doi.org/10.1016/j.soildyn.2021.107115

Link to publication on Research at Birmingham portal

General rights
Unless a licence is specified above, all rights (including copyright and moral rights) in this document are retained by the authors and/or the copyright holders. The express permission of the copyright holder must be obtained for any use of this material other than for purposes permitted by law.

•Users may freely distribute the URL that is used to identify this publication.
•Users may download and/or print one copy of the publication from the University of Birmingham research portal for the purpose of private study or non-commercial research.
•User may use extracts from the document in line with the concept of 'fair dealing' under the Copyright, Designs and Patents Act 1988 (?)
•Users may not further distribute the material nor use it for the purposes of commercial gain.

Where a licence is displayed above, please note the terms and conditions of the licence govern your use of this document.

When citing, please reference the published version.

Take down policy
While the University of Birmingham exercises care and attention in making items available there are rare occasions when an item has been uploaded in error or has been deemed to be commercially or otherwise sensitive.

If you believe that this is the case for this document, please contact UBIRA@lists.bham.ac.uk providing details and we will remove access to the work immediately and investigate.

Download date: 19. Apr. 2024

Local buckling behaviour of high-strength steel tubular columns subjected to one-sided cyclic loading and implications in seismic design of steel MRFs

Shingo Hamauzu[1,2,3], Konstantinos Skalomenos[1,2,*], Masahiro Kurata[1], Marios Theofanous[2]

[1]Disaster Prevention Research Institute, Kyoto University, Gokasho, Uji-shi, Kyoto 611 0011, Japan

[2]Department of Civil Engineering, University of Birmingham, Edgbaston, Birmingham B15 2TT, UK

[3]Takenaka Corporation, 4-1-13, Honmachi, Chuo-ku, Osaka 541 0053, Japan

Abstract: *After yielding, steel structures progressively exhibit an asymmetrical hysteretic behaviour under earthquakes biased in one direction (ratcheting effect). This response may be favourable to structural components because of the absence of symmetrical cyclic loading reversals. To evaluate the inelastic behaviour of components to asymmetrical cyclic loading, this study develops a set of one-sided cyclic loading histories for columns on the basis of a parametric study on the asymmetrical hysteretic behaviour of steel moment-resisting-frames (MRFs). Experimental and computational results indicate that steel tubular columns subjected to one-sided cyclic loading may exhibit 15% to 71% higher ductility compared with that under symmetrical cyclic loading showing adequate resistance to local buckling initiation and sufficient ductility afterwards. These reduced ductility demands may permit the use of high-strength steels in energy dissipative zones, such as high yield-to-tensile strength ratio (Y/T) steels, resulting in reduced material consumption and more economical seismic design of buildings. The above findings are utilised in the seismic design of a MRF employing high Y/T steel, which enjoys almost the same lateral strength as a corresponding conventional steel MRF but nearly 25% smaller cross-sectional area in columns. Nonlinear time-history analyses revealed that the high Y/T MRF behaved elastically under frequent events, whilst the ground floor columns of the conventional MRF yielded. Under rare seismic events, the average story drift ductility demand for the high Y/T MRF was only 1.77, while for the conventional MRF was 2.57. The former MRF successfully resisted the earthquake loads without experiencing local buckling in columns.*

Keywords: Steel MRFs, High *Y/T* steels, Square tubular columns, One-side cyclic loading, Local buckling

[*]Correspondence email: k.skalomenos@bham.ac.uk

1 Introduction

Current seismic design codes do not permit the use of high-strength steels in energy dissipative zones of steel structures, as their inferior strain-hardening characteristics and relatively low ductility may lead to premature failure under cyclic loading [1]. Relevant upper limits in yield stress of structural steels, including limitations for the yield-to-tensile strength ratio (*Y/T*) (high-strength steels provide high *Y/T* ratio), have mainly been established or assessed by subjecting individual structural components to displacement loading histories that impose the seismic ductility demands quasi-statically. The most widely used loading histories are conventional cyclic loading protocols consisting of symmetrical positive and negative cyclic displacement reversals (ATC, SAC, FEMA) [2-6] (Figure 1a). However, full-scale shaking table experiments have shown that steel structures progressively exhibit an asymmetrical nonlinear hysteretic response after yielding, predominantly in one direction, without a corresponding unloading in the other direction [7]. The resulting nonlinearities are then biased in one direction (one-sided hysteretic behaviour) creating a stepwise ratcheting effect [8] (Figure 1a). This effect may result in reduced ductility demands for individual components because of the absence of symmetrical cyclic reversals [9]. This paper aims to investigate the one-sided hysteretic behaviour of tubular steel columns giving an emphasis to simulate the progressive damage accumulation caused by the gradual yielding of structures and local buckling growth. Then it will explore whether the more susceptible to local buckling high *Y/T* steel columns can be used in energy dissipative regions of steel structures.

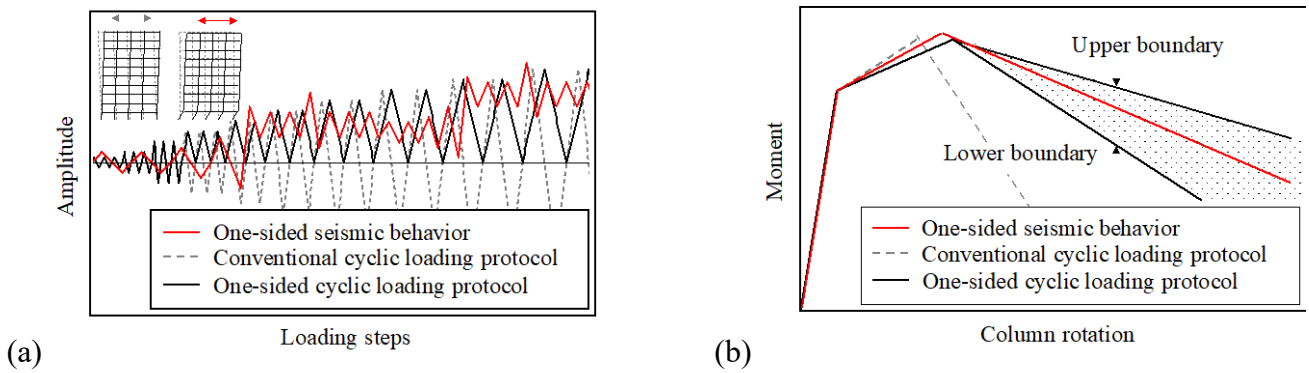

Figure 1 a) One-sided cyclic behaviour; b) Backbone curves of the normalized *M-θ* relationship (illustration of the lower and upper *M-θ* capacity bounds under conservative and non-conservative one-sided loading histories, respectively, based on findings of this study)

Ghassemieh et al. [10] have recently reported the strong influence the loading protocol sequence has on quantifying the seismic capacity of structures through various evaluation indices, such as the energy dissipation, equivalent plastic strain, and deformation capacity, in accordance with design level and near collapse earthquakes. Krawinkler et al. [11, 12] introduced typical loading protocols for steel beam-to-column subassemblies that contain the design level seismic demand (symmetrical protocols) and the effect of large displacement pulses (typical one-sided protocols). Among these, the *SAC Near-Fault protocol* simulates the one-sided cyclic behaviour of structures but emphasizes the behaviour incipient to collapse. In fact, the pulse-type loading amplitudes and large reversals of near-fault protocols abruptly drive the structures into the inelastic region and may not always realistically describe the progressive transition from the initial symmetrical hysteretic behaviour to the one-sided hysteretic behaviour as dictated by the stepwise damage growth. In latter case, a gradual exhaustion of ductility capacity is expected to take place as has been seen under repeated earthquakes or earthquake sequences of design-basis or major events [8, 13-19]. Research findings herein, clearly indicate the need to include cyclic loading histories that impose a progressively repeated one-sided damage accumulation which is more demanding than that corresponding to the current collapse-consistent loading protocols (e.g., SAC Near-Fault protocol) and less demanding than that corresponding to the codified symmetrical loading protocols (e.g., SAC protocol).

Loading protocols that combine one-sided asymmetrical cyclic patterns have been studied for structural steel, concrete and timber elements suggesting that one-sided cyclic and/or monotonic tests may be more representative in simulating the inelastic seismic demands on buildings [20-24]. The inelastic capacity of members evaluated under these loading protocols was found to be higher than the one under the codified symmetrical loading protocols suggesting a new direction in setting strength and ductility limits for the design of components. Some of these loading protocols account for the various design characteristics of the buildings (building height, span, cross-sectional width-to-thickness ratio and strong-column weak-beam ratio) and have been developed on the basis of a number of collapse-inducing seismic loads. However, the above protocols do not account for a progressive one-sided damage accumulation of the inelastic

response, thus provide relatively similar results to *SAC Near-Fault protocol*.

Analyses in previous studies were performed utilizing spring-based models, and in some cases generalized SDOF systems. For simplicity and practicality, cyclic/in-cycle degradation effects were either entirely neglected, or if at all considered, they were assumed to be controlled by loading history independent parameters (e.g., predefined deterioration), which had been previously calibrated against tests or analyses of components subjected to symmetrical cyclic loading histories (e.g., Ref [7, 25]). The accumulation of damage manifesting as global strength and stiffness deterioration under one-sided asymmetrical loading, which appears to be more realistic for structural components, has not been investigated through load dependent distributed plasticity models (i.e., detailed finite element (FE) methods of full-scale MDOF systems. Ideally, this modelling approach can trace the stepwise damage growth with less uncertainty, as well as provide a sufficient information for the intermediate area of the hysteretic response. This will enable a better quantification of the ductility demands under one-sided loading protocols with special focus on assessing localized failures in structures, such as local buckling initiation and post-peak strength deterioration (i.e., post-local buckling response).

This paper investigates the asymmetrical hysteretic behaviour of tubular steel columns and aims to quantify the ductility and post-peak strength capacity they possess when subjected to the more favourable and realistic one-sided cyclic loading protocols. Findings of this investigation are then reflected into the seismic design of steel moment-resisting-frames (MRFs) where a high *Y/T* steel is utilized in columns. To achieve this aim, the present study has developed the following original methodical steps:

1) A seismic response databank of typical steel MRFs with square tubular steel columns and H-beams is created through detailed FE load-dependent distributed plasticity models [26] of full scale MDOF systems that can actively trace the one-sided global hysteretic response. The frame FE models include all necessary material and local/global geometrical nonlinearities to explicitly capture strength and stiffness degradation due to local buckling. Different design characteristics, such as the beam-to-column moment ratio at joints and the axial loads in columns, are considered.

2) A new computational method is proposed to identify the one-sided global plastic mechanisms of the

frames by implementing the principles of the sequential earthquake analysis [13-19]. The designed MRFs are subjected to repeated earthquake motions imposing gradual one-sided asymmetrical deformations on the structures thus allowing the corresponding global one-sided plastic mechanism of frames to be accurately identified. This allows the evaluation of the one-sided stepwise damage growth under repeated loading which may not be always captured under collapse-inducing seismic loads.

3) On the basis of the seismic response database of the steel MRFs, several sets of one-sided cyclic loading histories are developed and categorized, as shown in Figure 1a, with respect to well-known local and global evaluation indices for loading protocols, such as the number of loading cycles (N_t), the maximum drift (θ_{max}), the maximum drift ranges ($\Delta\theta_{max}$) and the cumulative plastic drift (CPD).

4) The experimental asymmetrical cyclic response of square tubular steel columns is investigated. Then, a large database with the inelastic responses of columns made of both conventional and high *Y/T* steels is developed by subjecting column FE models to the one-sided loading histories. This approach led to a new and more realistic definition of a lower and upper bound of the moment-rotation (M-θ) capacity curves of the columns shown in Figure 1b, as instructed by the asymmetry (i.e., level of conservatism) of each cyclic loading history. On the basis of the column response database, the current plastic and compact classification limits for steel tubular columns in design codes [27-32] are reassessed.

5) Finally, the findings are translated into steel MRFs seismic demands. The seismic performance of a newly designed MRF with columns made of conventional steel and high *Y/T* steel is investigated through nonlinear time-history analyses under ground motions compatible to two Japanese hazard levels (Level 1 earthquakes that correspond to a return period of 50 years, and Level 2 earthquakes that correspond to a return period of 500 years, approximately). Comparisons are made with respect to the onset of yielding, local buckling initiation and story drift ductility demands.

2 Asymmetrical seismic behaviour of steel MRFs

2.1 Parametric study and analysis procedure

The asymmetrical hysteretic behaviour of steel moment-resisting-frames (MRFs) is investigated by

performing time-history finite element (FE) analyses using full-scale plane frame models. The parametric study is conducted in a cloud cluster supported by a super-computer (HPC) facility [33]. Originally, a three-dimensional (3D) 5-story and 3-span office building is designed according to Japanese seismic design code as a reference structure [34]. Figure 2a shows the elevation and plan view of the reference 3D building. One plane frame of this building is modelled with the aid of the finite element analysis software ABAQUS [26]. Figure 2b illustrates an overview of the frame FE model. The frame model developed herein is a mixed shell/beam element frame model that combines the powerful nonlinear S4R shell elements employed to discretise the critical regions of the building, such as beam-to-column connections and columns at the base where cross-sectional instabilities (e.g., local buckling) are expected, with the B31 Timoshenko beam-column elements which were employed to discretise the remaining structure in non-critical regions [35]. The boundary nodes between beam and shell elements are connected through multi-point constraints (type beam). The beam-to-column connection is fully restrained by diaphragm plates located at the bottom and top of the panel-zone height thus simulating a rigid welded connection. The weld access hole is not modelled. Shell elements are used for a length equal to twice the width of column and beam depth, respectively, in order to accurately capture the local buckling initiation and post-local buckling response (plastic hinge zone). It has been observed in previous experiments and detailed finite element analyses that this is an adequate length for the formation of the plastic hinge [25]. For sufficiently small strains, steel is modelled as a linear elastic isotropic material with density ρ = 7,850 kg/m^3, modulus of elasticity E = 205GPa and Poisson's ratio v = 0.3. For large strains, this constitutive model includes von-Mises yield criterion with kinematic hardening and is suitable to simulate the inelastic behaviour of metals under cyclic loading (combined isotropic-kinematic hardening model). In this parametric study of steel MRFs, a strain hardening slope of 1.0% of the modulus of elasticity was assumed as recommended in EN 1993-1-5 [36]. This value has been found to be conservative for some cases [37] but suitable for performing global inelastic seismic analysis in steel framed structures [28, 38]. Using actual material response characteristics as obtained from material coupon tests is expected to lead to more reliable predictions of the structural performance, however the applicability of the results will be strictly restricted to structures employing the material that was tested. Hence, it was decided to employ a more simplified and slightly conservative

material response following code recommendations.

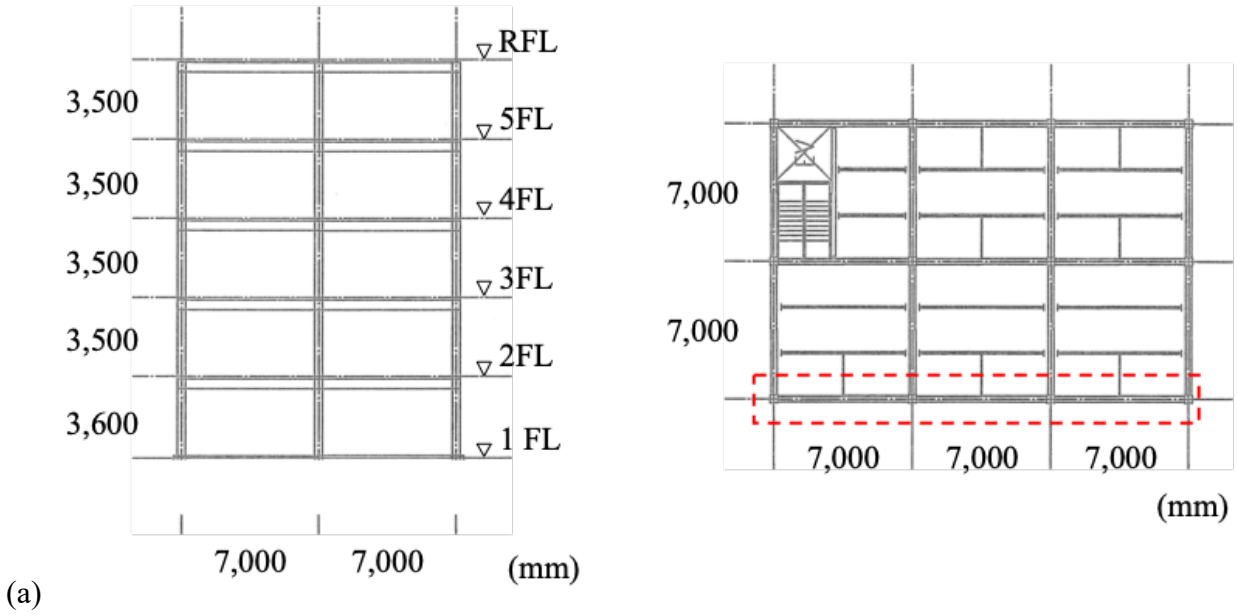

(a)

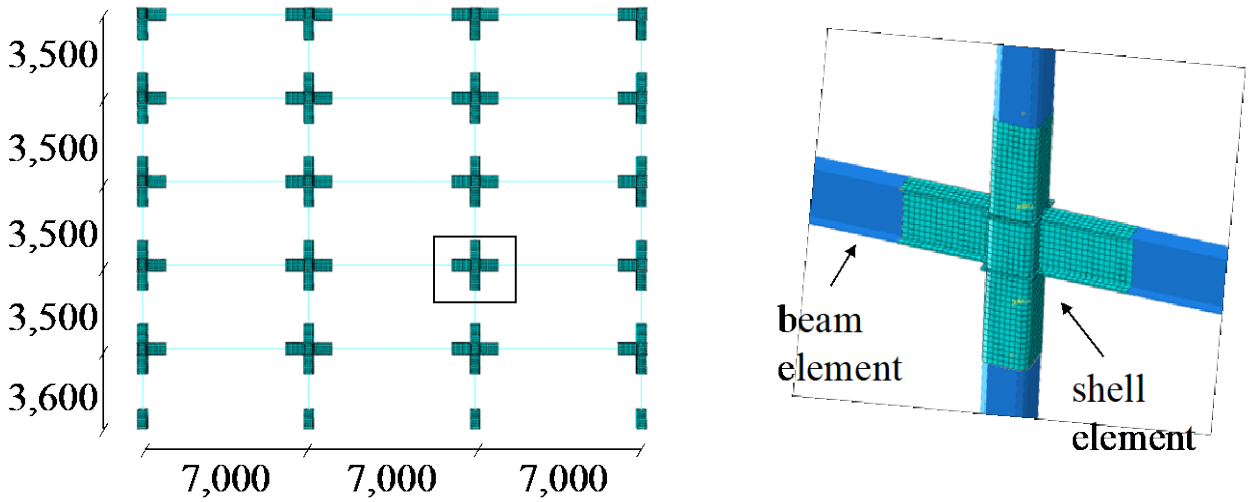

(b)

Figure 2 Structure model: a) elevation and plan view of the 3D steel MRF (mm) [34]; b) FE model of the plane frame as developed in ABAQUS [26]

Table 1 lists the geometric, design and dynamic characteristics for the reference building including gravity loads. The gravity loads are applied as concentrated loads on the external and internal joints of the frame. The fundamental natural period of the plane frame is 0.83 sec. The lateral story drift profile [i.e., 0.38, 0.50, 0.47, 0.41, 0.31] was found to be almost identical with the drift profile of the reference 3D building structure [34], as this was obtained under the A_i seismic load distribution [28] and a base shear coefficient C_0 = 0.20. Regarding the cross-sections of the frame members, the columns are cold formed square hollow sections (SHS) made of steel grade BCR295 (yield stress f_y = 295 MPa) and the beams are

H-shaped sections made of the steel grade SN400B (yield stress f_y = 235 MPa). The moment strength ratio between the total plastic moment of columns ($\Sigma M_{p,c}$) and the total plastic moment of beams ($\Sigma M_{p,b}$) ($= \Sigma M_{p,c}/\Sigma M_{p,b}$) at the joints of the 1st story (i.e., ground floor) is equal to 1.2. For the parametric study, two additional plane MRFs with moment ratios equal to 1.6 and 2.0 are designed by changing column thickness, as shown in Table 1. The fundamental natural period of the frames varies when increasing the column wall thickness from 0.83 to 0.74 sec. Table 2 reports the employed column and beam cross-sections at each story of the structure. The corresponding ground floor moment ratio of each steel MRF is presented as reference value (i.e., 1.2, 1.6 and 2.0). Two axial load ratios ($n = N/N_y$; where N_y is the yielding axial strength of the columns) equal to 0.12 and 0.24 are considered. Preliminary nonlinear static analysis (pushover analysis) is performed to identify the global plastic mechanism for each frame model, as shown in Figure 3 and discussed in Table 2 following the A_i load distribution. One can clearly observe the influence of the moment ratio and axil ration on the global failure mechanism which may involve: (a) all the stories (ALL), (b) the 1st story to 3rd story (1-3 story) and (c) the 2nd story and 3rd story (2-3 story) of the structure.

For the time-history analysis, four ordinary and unscaled ground motion records are selected from the PEER Ground Motion Database [39]. Figure 4 compares the response spectrum of each ground motion with the elastic spectrum. The selected ground motions are the *El centro H1,* the *El centro H2*, *Takarazuka* and *Takatori*. It should be noted here that the ground motions are compatible to 1.5 times the Japanese elastic spectrum [28] for the range of the fundamental natural period T_1 from $0.2T_1$ to $2.0T_1$. The proposed set of the ordinary ground motions (unscaled) compatible to 1.5 times the elastic response spectrum is found to be sufficient to lead all steel MRFs to significant inelastic response.

Table 1 Design and dynamic characteristics of the steel MRFs considered in the parametric study

Office building [34]	
Height, h [mm]	17,600
Span, L [mm]	7,000
Story height, H [mm]	3,500
Fundamental period, T [sec]	0.83 (0.78, 0.74)
$\Sigma M_{p,c}/\Sigma M_{p,b}$	1.2 (1.6, 2.0)
Axial load ratio, n	0.12 / 0.24
Base shear coefficient	0.55
Steel grade for columns	BCR295 (f_y = 295 MPa; f_u = 400 MPa)
Steel grade for beams	SN400B (f_y = 235 MPa; f_u = 400 MPa)

Floor gravity loads external / internal columns [kN], n = 0.12	105.5 / 211.0
Top floor gravity loads external / internal columns [kN], n = 0.12	128.0 / 256.0

Table 2 Design and characteristics of the three steel MRFs: Cross-sections of the members, column-to-beam moment ratios, axial load ratios and stories involved in the global plastic mechanisms

MRF	Story	Column (D/t)	Beam	$\Sigma M_{p,c}/\Sigma M_{p,b}$	$n\ (=N/N_y)$	Stories involved in plastic mechanism
1	1st 2nd 3rd-5th	SHS−400×400×16[a] (25) SHS−400×400×14 (29) SHS−400×400×12 (33)	H−500×300×11×18[b] H−500×200×10×16 H−500×200×10×16	1.2[c]	0.12 / 0.24	1-3 / 2-3
2	1st 2nd-5th	SHS−400×400×19 (21) SHS−400×400×19 (21)	H−500×300×11×18 H−500×200×10×16	1.6	0.12 / 0.24	1-3 / 1-3
3	1st 2nd-5th	SHS−400×400×25 (16) SHS−400×400×25 (16)	H−500×300×11×18 H−500×200×10×16	2.0	0.12 / 0.24	ALL / ALL

[a]400×400×16: width× width ×thickness
[b]500×300×11×18: height × width × web thickness × flange thickness
[c]calculated for the 1st story (ground floor)

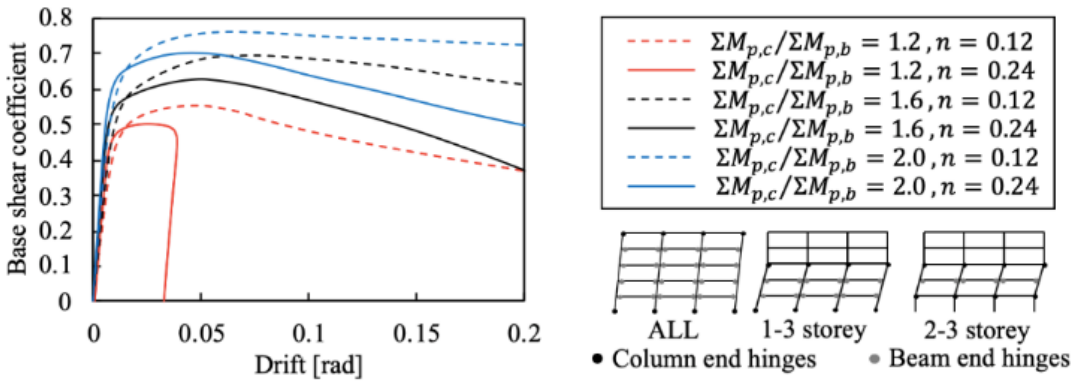

Figure 3 Pushover curves and global plastic mechanisms

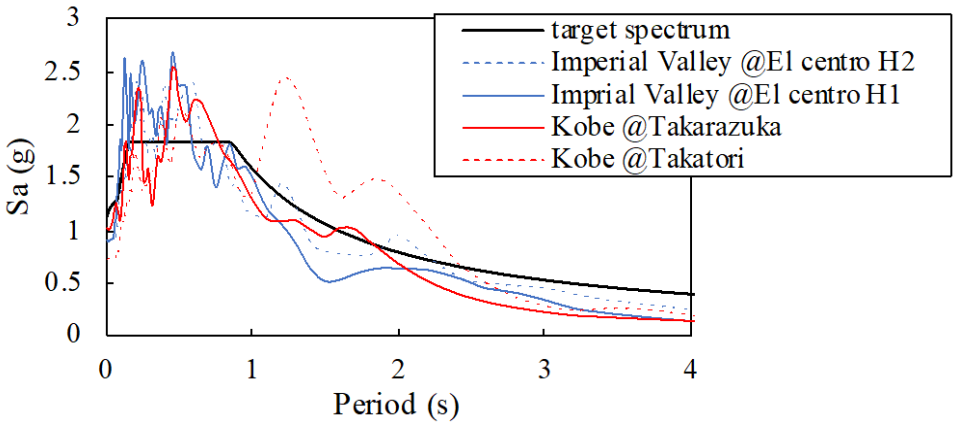

Figure 4 Comparison of the acceleration spectra of selected ground motions to 1.5 times the Japanese

elastic response spectrum [28]

The selected ground motions are applied (unscaled) three times with a 100 sec gap in between each application, as shown in Figure 5, thus allowing the free oscillation of the frame between the successive seismic applications to cease [19, 40]. This analysis procedure can successfully drive the structures to one-sided global failure mechanisms (Figure 3) tracing the gradual transition from the yielding state to the asymmetrical global instability. The repetition of the seismic motion by three times in this study was found to be adequate to impose the target cumulative plastic drift (CPD) and target maximum drift (θ_{max}) on the column members, both necessary quantities for the characterization of the one-sided loading histories as discussed later. Figure 5 shows the acceleration time-history for the repeated Takatori ground motion, as a representative example, while Table 3 summarizes all analysis cases considered in the parametric study. The name of each analysis begins with the indication of the moment ratio at frame joints (e.g., "R12" corresponds to a $\Sigma M_{p,c}/\Sigma M_{p,b}$ = 1.2), followed by an indication of the axial load ratio in columns (e.g., letter "N" corresponds to an n = 0.12 while letter "2N" corresponds to an n = 0.24), an ending by an indication of the applied ground motion (e.g., "H1" indicated the "*Imperial Valley @El centro H1*").

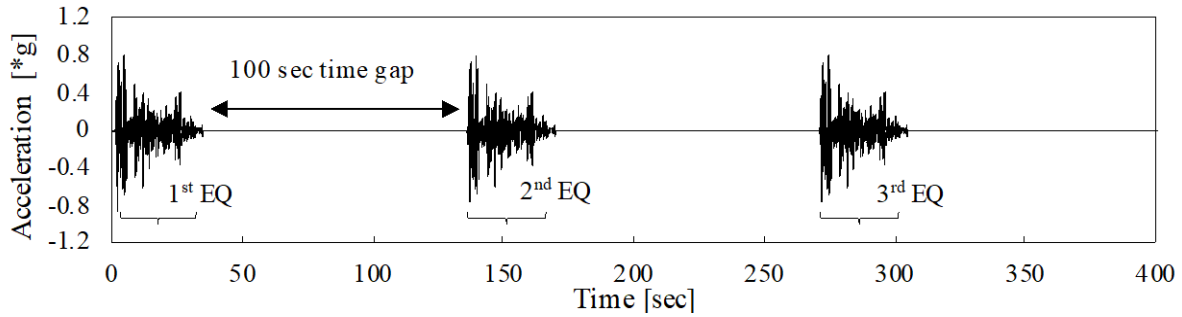

Figure 5 Three times repeated acceleration time history (*Takatori*) with 100 sec time gap

Table 3. Analysis cases of the parametric study

Analysis case	Name	$\Sigma M_{p,c}/\Sigma M_{p,b}$	n	Ground motion
1	R12_N_ H1	1.2	0.12	Imperial Valley @El centro H1
2	R12_N_ H2	1.2	0.12	Imperial Valley @El centro H2
3	R12_N_zuka	1.2	0.12	Kobe@Takarazuka
4	R12_N_tori	1.2	0.12	Kobe@Takatori
5	R16_N_ H1	1.6	0.12	Imperial Valley @El centro H1
6	R16_N_ H2	1.6	0.12	Imperial Valley @El centro H2
7	R16_N_zuka	1.6	0.12	Kobe@Takarazuka

8	R16_N_tori	1.6	0.12	Kobe@Takatori
9	R20_N_ H1	2.0	0.12	Imperial Valley @El centro H1
10	R20_N_ H2	2.0	0.12	Imperial Valley @El centro H2
11	R20_N_zuka	2.0	0.12	Kobe@Takarazuka
12	R20_N_tori	2.0	0.12	Kobe@Takatori
13	R12_2N_ H1	1.2	0.24	Imperial Valley @El centro H1
14	R12_2N_ H2	1.2	0.24	Imperial Valley @El centro H2
15	R12_2N_zuka	1.2	0.24	Kobe@Takarazuka
16	R12_2N_tori	1.2	0.24	Kobe@Takatori
17	R16_2N_H1	1.6	0.24	Imperial Valley @El centro H1
18	R16_2N_H2	1.6	0.24	Imperial Valley @El centro H2
19	R16_2N_zuka	1.6	0.24	Kobe@Takarazuka
20	R16_2N_tori	1.6	0.24	Kobe@Takatori
21	R20_2N_H1	2.0	0.24	Imperial Valley @El centro H1
22	R20_2N_H2	2.0	0.24	Imperial Valley @El centro H2
23	R20_2N_zuka	2.0	0.24	Kobe@Takarazuka
24	R20_2N_tori	2.0	0.24	Kobe@Takatori

2.2 Repeated time-history analysis results

Figure 6 presents representative time-history analysis results of steel MRFs (analysis cases 1, 2, 3 and 4, as shown in Table 3) in terms of base shear coefficient - story drift relationship and the associated drift time-history of the 1st story (ground floor). Among the four ground motions considered, the *Takatori* ground motion (analysis case 4) caused the most severe damage, and a significant stepwise growth of the residual story drift was observed toward one direction. This frame reached a maximum story drift equal to 0.074 rad and a residual story drift equal to 0.029 rad. In the corresponding analysis case that assumes an axial load ratio of $n = 0.24$ (analysis case 16), a more intensive on-sided asymmetrical hysteretic behaviour was observed due to greater axial loads. Figure 7a visually illustrates the stress distribution and the yielded areas, hence plastic hinge locations (light grey indicates yielding), for analysis case 16 (*R12_2N_tori*). Time-history results of the associated base shear coefficient and story drift are illustrated in Figure 7b. According to the preliminary pushover analysis, as shown in Figure 3, this frame was expected to exhibit a soft story failure mechanism that involves the formation of a plastic mechanism between the 2nd and 3rd story. However, the time-history analysis predicted a different overall failure mechanism that involves the 1st story and the 3rd story. One can observe in Figure 7b the asymmetric growth of inelastic sway deformations of the frame in one direction and the corresponding strength degradation once local buckling of the column members has occurred at the ground level and the 3rd story, respectively. The results

of this section clearly indicate the effectiveness of the proposed analysis procedure that utilizes repeated earthquakes to trace the one-sided asymmetrical hysteretic behaviour of steel MRFs. The influence of critical design parameters of the steel MRFs, such as the joint moment ratio and the column axial load ratio, are successfully assessed.

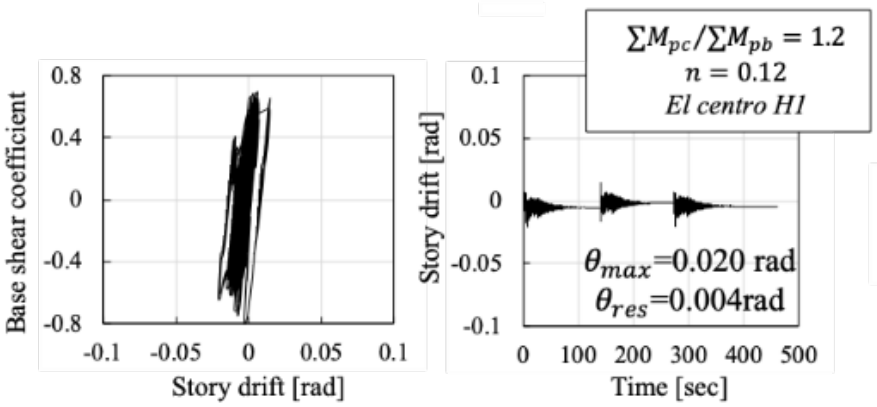

(a)

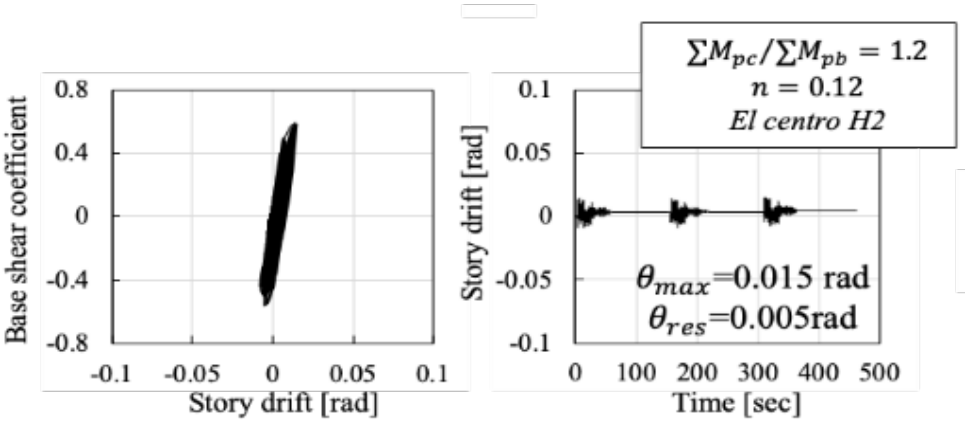

(b)

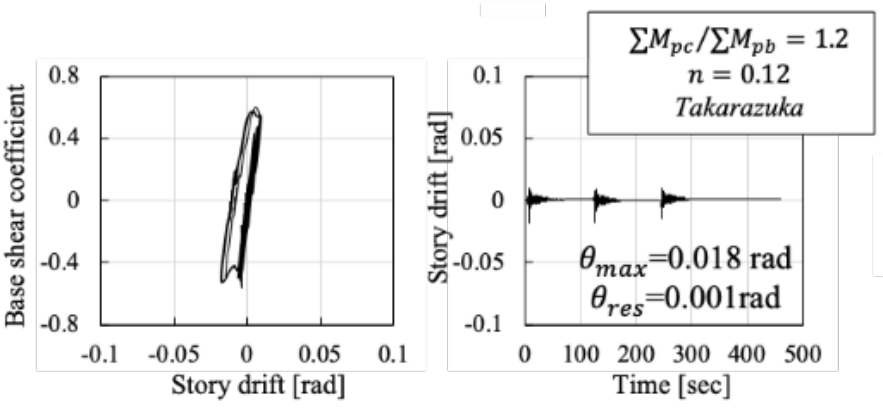

(c)

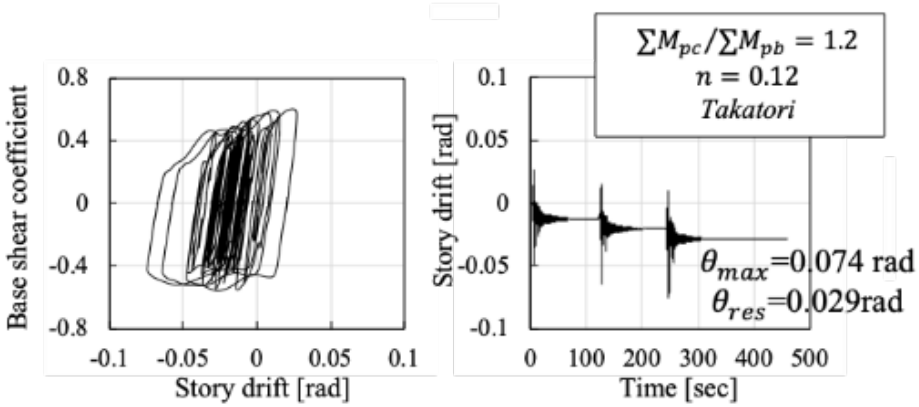

(d)

Figure 6 Story drift vs base shear relationship along with the drift time-history of the 1st story for: (a) *R12_N_H1* (analysis case 1); (b) *R12_N_H2* (analysis case 2); (c) *R12_N_zuka* (analysis case 3); and (d) *R12_N_tori* (analysis case 4)

220

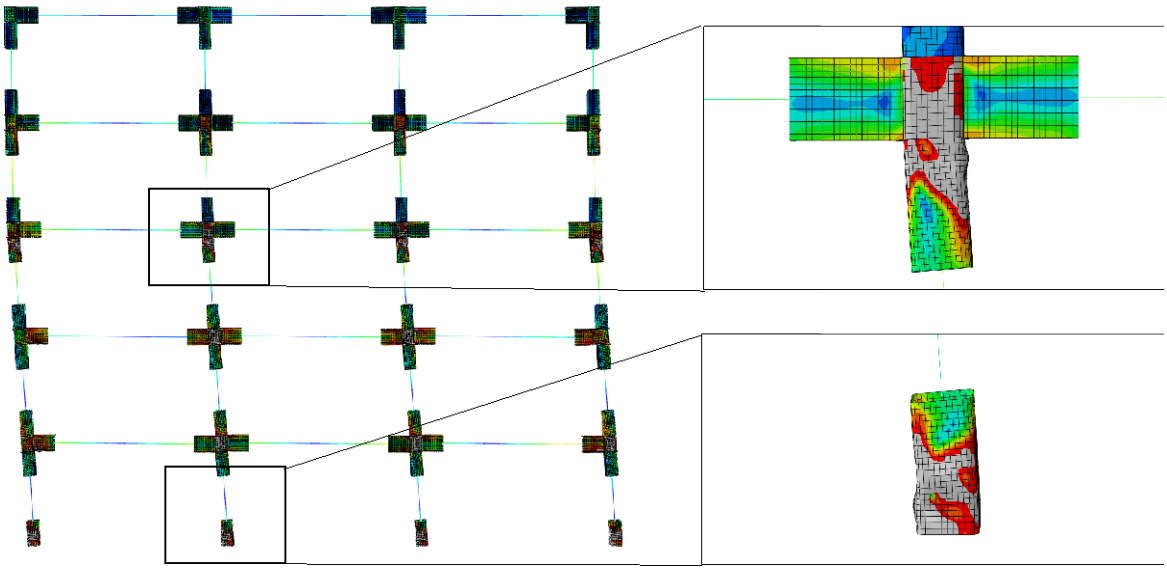

(a)

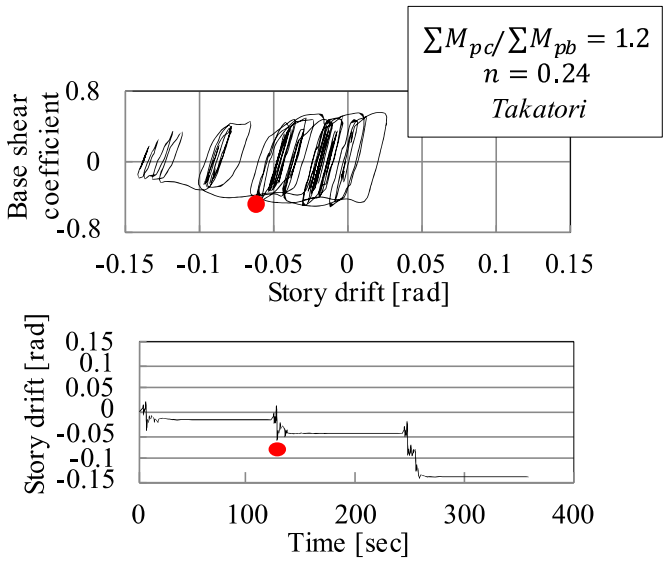

(b)

Figure 7: One-sided seismic behaviour of the analysis case 16 (*R12_2N_tori*): (a) failure of local buckling at the base of the 1st story columns and the top of the 3rd story columns during the second repeated ground motion; (b) base shear coefficient – 1st story drift relationship and drift time-history of the 1st story.

3 Development of the one-sided loading histories

3.1 Cyclic loading histories

Various conventional cyclic loading protocols have been developed so far aiming at imposing a cumulative cyclic damage to the structural components [2-6, 11, 12]. The total number of loading cycles and the amplitude of each loading cycle greatly affect the cumulative damage. The *SAC loading protocol* developed for steel structures [2, 11, 12] consists of six repeated symmetric cycles of relatively low amplitude which are imposed before the onset of component yielding, followed by repeated sets of two loading cycles of gradually increasing amplitude. These sets of repeated cycles are imposed to drive the component into its inelastic region of response. This loading pattern of equal positive and negative reversals is repeated until the ultimate failure of the component. Compared to the one-sided asymmetrical response discussed previously, the current symmetric cyclic loading may impose excessive cumulative damage to the components for a given maximum deformation, as shown in Figure 8, thus overestimating the strength and ductility demands that the component will experience during earthquakes. On the basis of the previous section, steel structures subjected to earthquakes may reach larger deformations in conjunction with smaller

cumulative damage, thereby exhibiting a higher strength and ductility than the one determined based on a conventional symmetric cyclic loading protocol.

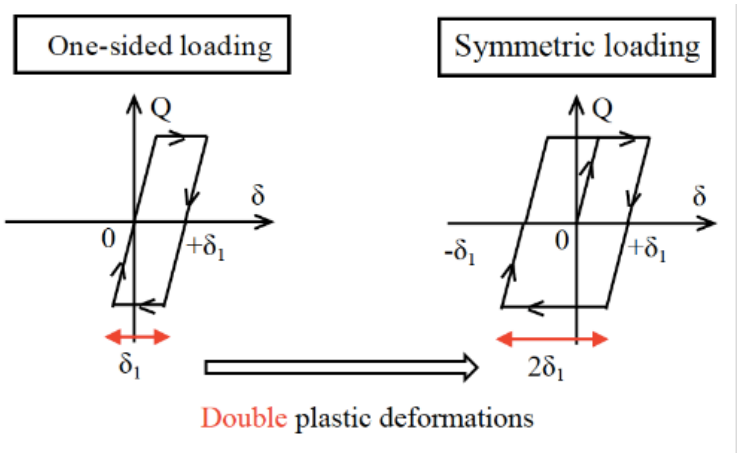

Figure 8 Deformation demands imposed by symmetric and one-sided cyclic loading histories

3.2 Asymmetrical cyclic loading histories

3.2.1 Current collapse-consistent loading protocols

Krawinkler [12] summarized a few symmetrical and asymmetrical loading protocols including the *SAC loading protocol* and the *SAC Near-Fault protocol*, respectively. The *SAC Near-Fault protocol* aims to evaluate the performance of structures subjected to collapse-inducing seismic loads, such as pulse-type ground motions. The *SAC Near-Fault protocol* is adopted in this study as an example of asymmetrical lading histories alongside with a second *collapse-consistent protocol* [22-24] that accounts for the design characteristics of a 5-story steel structure (H=18.4m) with a moment ratio equal to 1.6 and steel SHS columns with width-to-thickness ratio *D/t* equal to 21.9. Both protocols impose large pulse reversals, as shown in Figure 9, and simulate collapse of steel structures.

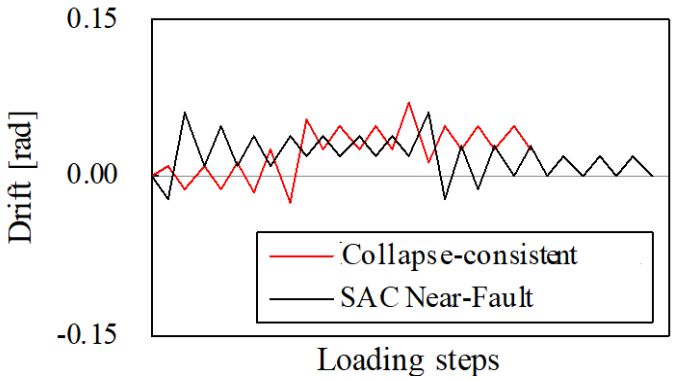

Figure 9 Collapse-consistent loading protocols

As stated in the introduction, the pulse-type loading amplitudes of collapse-consistent protocols may not be always accurate in simulating the one-side hysteretic behaviour of structures subject to ordinary ground motions at the level of a design-basis or major earthquake event. In addition, the large amplitudes of their reversals may dominate the loading history at each damage state producing a response which is relatively close to the monotonic response of the structure, thus imposing relatively low seismic demands. This is in accordance with Refs [11, 24] which state that monotonic tests are often adequately to simulate the inelastic seismic demands at collapse. This study aims to quantify the one-side hysteretic behaviour of structures that are first subjected to a few symmetrical elastic and inelastic cycles and then to several asymmetrical inelastic cycles that produce a progressive development of damage predominantly in one direction. This loading pattern will be more demanding than the current collapse-consistent loading protocols and less demanding than the codified symmetrical loading protocols.

3.2.1 Developed one-sided loading protocols

The conventional *SAC protocol* [2] has widely been used to investigate the deformation capacity and the cyclic deterioration of steel columns. In this study, one-sided cyclic loading histories are developed on the basis of the conventional *SAC protocol* with some modifications. Four different types of asymmetric loading patterns are developed by modifying the parameters of the *mean drift*, *maximum drift*, *maximum drift range*, and *number of loading cycles* of conventional *SAC protocol*. All types of one-sided loading patterns considered are described below, while the corresponding loading histories are illustrated in Figure

10, where the conventional *SAC protocol* is also shown for comparison. For the examined protocols, the one-sided hysteretic behaviour is assumed to initiate after reaching a story drift equal to 0.01 rad ($\theta_{init} = 0.01$ rad) that corresponds to the yield rotation of columns. In addition, a $\theta_{init} = 0.02$ rad is examined. In total 8 loading histories are created simulating different scenarios of one-sided seismic demands.

One-sided cyclic loading-1

This loading history, hereafter referred to as "*OD-1*", is generated by modifying the negative reversals of the conventional *SAC protocol* after the onset of yield drift θ_{init}. Figure 10a shows the *OD-1* loading history. The elastic part of this loading history is identical with that of the conventional protocol. The number of loading cycles and the amplitude of positive cycles are the same as the conventional protocol. After θ_{init}, the negative loading cycles constantly reach a negative value of θ_{init}. Based on previous shaking table tests [41], a two story and one span three-dimensional steel structure deformed in one direction after experiencing yielding reaching constantly an opposite story drift of -0.01 rad during the reversed amplitudes of the oscillation. Although H-sections were used for columns in this test, the primary failure mode was local buckling. The *OD-1* loading history simulates a conservative scenario of one-sided hysteretic behaviour driven by the positive maximum deformation of the conventional protocol.

One-sided cyclic loading-2

This loading history, hereafter called "*OD-2*", is the same as the *OD-1*, but the positive inelastic cycles are repeated four times instead of two times at each amplitude to compensate for the elimination of the negative maximum drifts. Figure 10b shows the *OD-2* loading history. When the maximum drift is imposed, an equivalent input energy with the full conventional *SAC protocol* will be achieved.

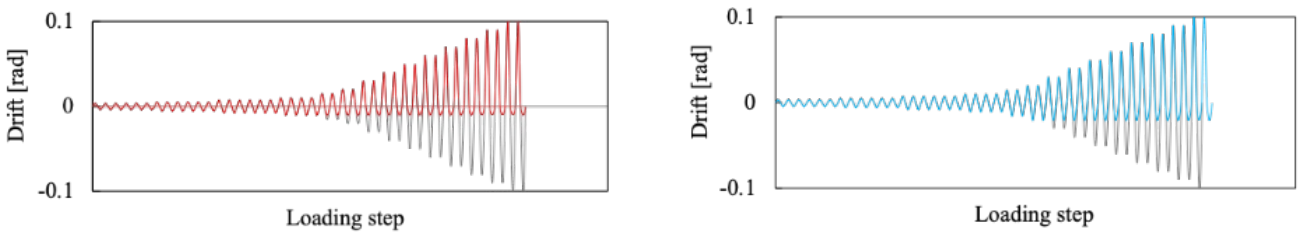

OD-1 ($\theta_{init} = 0.01$) OD-1 ($\theta_{init} = 0.02$)

(a)

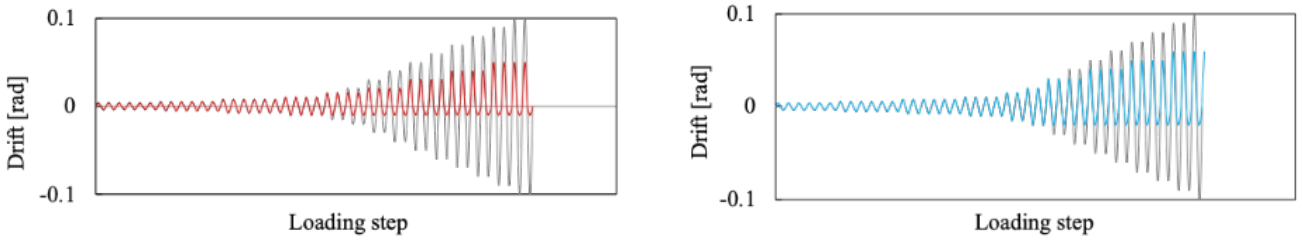

OD-2 ($\theta_{init} = 0.01$) OD-2 ($\theta_{init} = 0.02$)

(b)

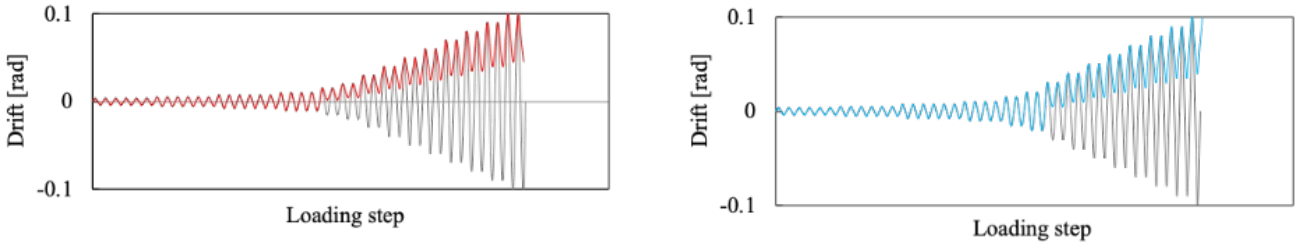

OD-3 ($\theta_{init} = 0.01$) OD-3 ($\theta_{init} = 0.02$)

(c)

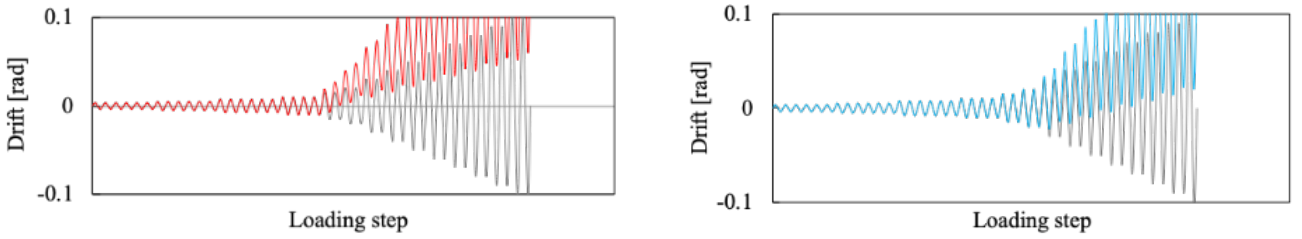

OD-4 ($\theta_{init} = 0.01$) OD-4 ($\theta_{init} = 0.02$)

(d)

Figure 10 (a) Developed one-sided cyclic loading histories under the assumption of θ_{init} = 0.01 and θ_{init} = 0.02 rad

288

289 ***One-sided cyclic loading-3***

290 This loading history, hereafter called "*OD-3*", has the same number of cycles and imposes an

291 identical maximum positive drift per loading cycle as the conventional *SAC protocol*. The negative

reversals have been completely removed and the oscillation takes place about a residual deformation that gradually increases, as shown in Figure 10c. In *OD-3* the selected inclination of the residual deformation is determined by the mean values of each drift cycle and has been set equal to the 60% of the maximum positive drift. Compared to *OD-1* and *OD-2*, *OD-3* is expected to reduce the demand for energy dissipation.

One-sided cyclic loading-4

This loading history, hereafter called "*OD-4*", is similar to *OD-3* and is driven by residual deformations, as shown in Figure 10d. For this loading scenario, the conventional *SAC protocol* has been inclined to produce asymmetry in loading cycles and consequently exceeds the maximum drift values of the symmetrical protocol. The number of loading cycles and the drift range are identical to the ones of the conventional protocol. The inclination of this protocol is based on the mean drifts which are equal to the 50% of the maximum drifts. Table 4 summarizes the number of loading cycles, the drift amplitudes, and the yield drift of each loading history.

Table 4 Data of loading protocols: number of loading cycles, drift amplitudes and yield drift of each loading history

Amplitude [rad.] - θ_{init} = 0.01											
OD-1			**OD-2**			**OD-3**			**OD-4**		
cycles	negative (-)	positive (+)	cycles	negative (-)	positive (+)	cycles	negative (-)	positive (+)	cycles	negative (-)	positive (+)
6	-0.00375	0.00375	6	-0.00375	0.00375	6	-0.00375	0.00375	6	-0.00375	0.00375
6	-0.005	0.005	6	-0.005	0.005	6	-0.005	0.005	6	-0.005	0.005
6	-0.0075	0.0075	6	-0.0075	0.0075	6	-0.0075	0.0075	6	-0.0075	0.0075
4	-0.01	0.01	4	-0.01	0.01	4	-0.01	0.01	4	-0.01	0.01
2	-0.01	0.015	4	-0.01	0.015	2	0.0025	0.015	1	-0.01	0.019
2	-0.01	0.02	4	-0.01	0.02	2	0.005	0.02	1	-0.007	0.027
2	-0.01	0.03	4	-0.01	0.03	2	0.01	0.03	1	0.001	0.04
2	-0.01	0.04	4	-0.01	0.04	2	0.015	0.04	1	0.004	0.048
2	-0.01	0.05	4	-0.01	0.05	2	0.02	0.05	1	0.012	0.066
2	-0.01	0.06	4	-0.01	0.06	2	0.025	0.06	1	0.01	0.074
2	-0.01	0.07	4	-0.01	0.07	2	0.03	0.07	1	0.018	0.092
2	-0.01	0.08	4	-0.01	0.08	2	0.035	0.08	1	0.016	0.1
2	-0.01	0.09	4	-0.01	0.09	2	0.04	0.09	1	0.024	0.118
2	-0.01	0.1	4	-0.01	0.1	2	0.045	0.1	1	0.022	0.126
Amplitude [rad.] - θ_{init} = 0.02											
6	-0.00375	0.00375	6	-0.00375	0.00375	6	-0.00375	0.00375	6	-0.00375	0.00375
6	-0.005	0.005	6	-0.005	0.005	6	-0.005	0.005	6	-0.005	0.005
6	-0.0075	0.0075	6	-0.0075	0.0075	6	-0.0075	0.0075	6	-0.0075	0.0075
4	-0.01	0.01	4	-0.01	0.01	4	-0.01	0.01	4	-0.01	0.01
2	-0.015	0.015	2	-0.015	0.015	2	-0.015	0.015	2	-0.015	0.015
2	-0.02	0.02	2	-0.02	0.02	2	-0.02	0.02	2	-0.02	0.02
2	-0.02	0.03	2	-0.02	0.03	2	0.005	0.03	1	-0.02	0.034
2	-0.02	0.04	2	-0.02	0.04	2	0.01	0.04	1	-0.022	0.042
2	-0.02	0.05	2	-0.02	0.05	2	0.015	0.05	1	-0.014	0.06
2	-0.02	0.06	2	-0.02	0.06	2	0.02	0.06	1	-0.016	0.068
2	-0.02	0.07	2	-0.02	0.07	2	0.025	0.07	1	-0.008	0.086
2	-0.02	0.08	2	-0.02	0.08	2	0.03	0.08	1	-0.01	0.094
2	-0.02	0.09	2	-0.02	0.09	2	0.035	0.09	1	-0.002	0.112
2	-0.02	0.1	2	-0.02	0.1	2	0.04	0.1	1	-0.004	0.12

306 ### 3.3 Evaluation indices of the one-sided hysteretic response

307 To evaluate the one-sided seismic demands imposed by each loading history, the relationship
308 between the mean drift and the total cumulative plastic drift (CPD) is considered. As shown in Figure 11,
309 the mean drift is calculated for each damaging cycle as the average value of the maximum and minimum
310 drifts and is a measure of the degree of one-sided sway deformations of the frame. The CPD is developed
311 progressively and calculated as:

312 $$\mathrm{CPD} = \sum_{i=1}^{N} \Delta\theta_{pi} \tag{1}$$

313 where N is the number of post-yielding cycles ($\Delta\theta > 0.01$ or 0.02) and the $\Delta\theta_{pi}$ is the plastic drift range.
314 Associating the CPD with the mean drift one can observe the level of asymmetry of each hysteretic
315 response.

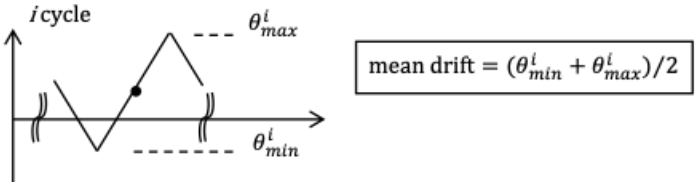

Figure 11 Definition of mean drift

316 Figure 12a depicts the relationship between the mean drift and the CPD for critical frame columns
317 as obtained from the full-scale FE time-history analysis of steel MRFs under the *Takatori* ground motion,
318 while Figure 12b depicts the same relationship under the other three ground motions. The columns with an
319 axial load ratio of n = 0.24 showed a greater propensity to asymmetrical sway response than the one with
320 an axial load ratio n = 0.12. The values of CPD varied with respect to the moment ratio at joints
321 ($\Sigma M_{p,c}/\Sigma M_{p,b}$) since the overall collapse mechanisms were found to also be affected by this ratio. For the
322 same mean drift, frames with a moment ratio equal to 2.0 reached CPD values beyond 0.5 rad whereas
323 frames with ratios equal to 1.2 reached values of CPD around 0.4 rad. Thus, the asymmetry of the one-
324 sided hysteretic behaviour of the frames increases as the moment ratio decreases. The frames with the lower
325 moment ratio appeared to be more sensitive to the ground motions reversals and the whipping effect was

pronounced more in these frames. One can observe this effect in the range of 0.05 to 0.15 CPD in Figure 12a.

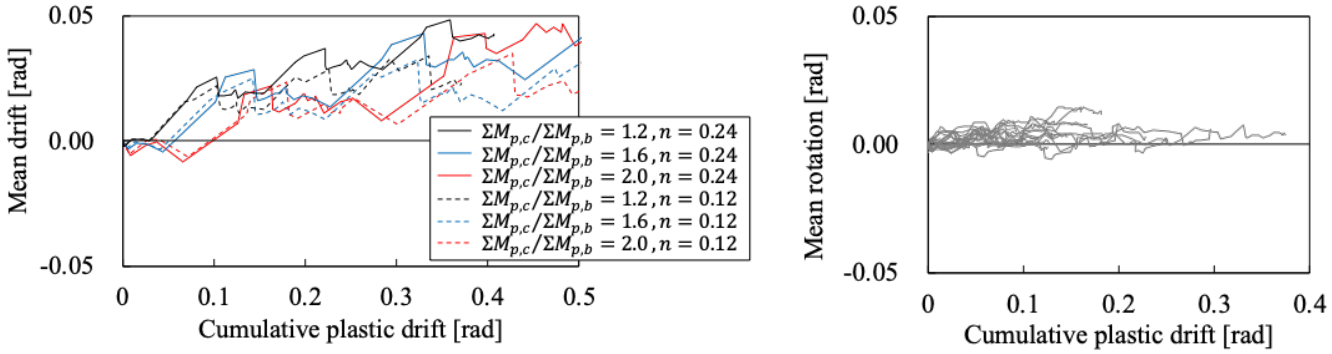

(a) (b)

Figure 12 Mean drift - CPD relationship of frame columns as obtained from the full-scale FE time-history analysis of steel MRFs: (a) under the *Takatori* ground motion, (b) under the other 3 ground motions

In addition to mean drift and CPD, other evaluation indices, such as, the number of loading cycles (N_t), the imposed maximum drift (θ_{max}), and the maximum drift ranges ($\Delta\theta_{max}$) are examined. The conventional *SAC protocol* typically consists of 30 loading cycles of stepwise increasing amplitude. This number may increase if a marked strength deterioration has not been observed by the end of the 30 loading cycles. When the 30 cycles are reached in the conventional protocol, θ_{max} = 0.04 and CPD = 0.49 rad for a yield rotation equal to 0.01 rad. Therefore, this value of CPD (= 0.5) is considered in this study as a threshold to evaluate N_t, θ_{max} and $\Delta\theta_{max}$ for the developed set of the one-sided loading histories. Figure 13a illustrates N_t when the CPD reaches 0.5 rad. The target value of N_t for the *SAC protocol* (illustrated as *SAC*) is 30. For the developed one-sided loading histories shown in Figure 10, N_t varies from 30 to 42 when CPD = 0.5 rad. On the contrary, in the *SAC Near-Fault protocol* (illustrated as *SAC N.F.*), N_t = 10, when CPD = 0.5 rad, as each cycle imposes a relatively large amplitude compared to the conventional symmetrical protocols. In principle, the proposed one-sided loading histories require greater N_t to impose a similar CPD to the one imposed by the conventional *SAC protocol* as they adopt smaller drift ranges.

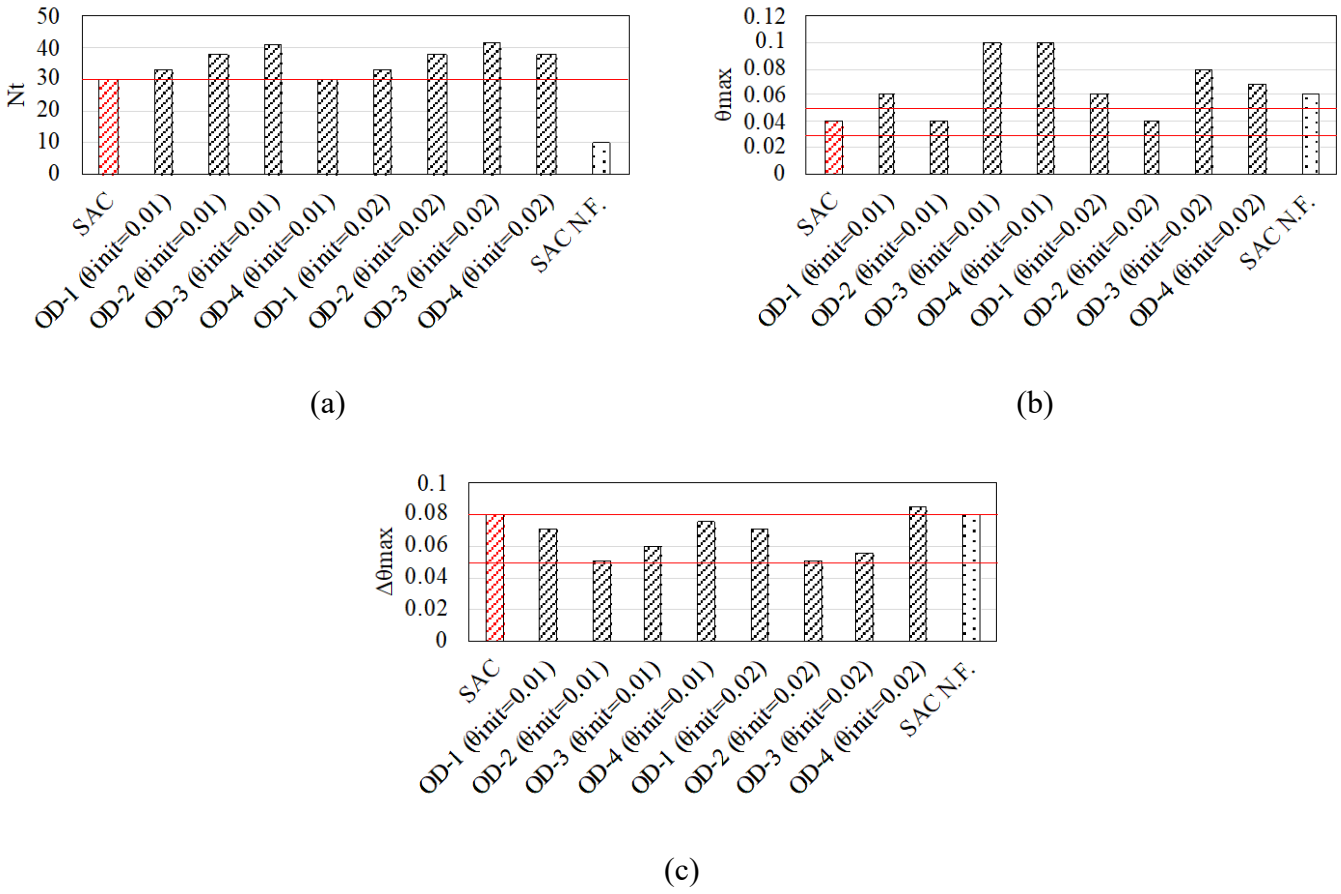

Figure 13 Key evaluation indices for the loading protocols when CPD = 0.5: (a) Number of cycles, N_t; (b) Maximum drift, θ_{max}; (c) Maximum drift range, $\Delta\theta_{max}$

The maximum story drift θ_{max} imposed by each protocol when CPD = 0.5 rad is illustrated in Figure 13b. Compared to the conventional *SAC protocol*, most of the developed one-sided loading histories impose a larger θ_{max}. The *SAC Near-Fault protocol* has one peak amplitude, which appears to be the θ_{max}. All other loading histories gradually reach θ_{max} and exhibit a pronounced one-sided hysteretic behaviour, particularly in case of *OD-3* ($\theta_{init} = 0.01$) and *OD-4* ($\theta_{init} = 0.01$). The target value of θ_{max} for the conventional *SAC protocol* was set 0.04 rad as an average between the 0.03 rad drift limit (i.e., earthquake having a 10% probability of exceedance in 50 years) and the 0.05 rad drift limit (i.e., earthquake having a 2% probability of exceedance in 50 years). Those two values were adopted in the SAC program as reference values associated with each seismic hazard and are plotted in Figure 13b (horizontal red lines). Same θ_{max} characterizes both the conventional *SAC protocol* and the *OD-2* ($\theta_{init} = 0.01, 0.02$) loading histories indicating similar cumulative damage despite the four repeated inelastic cycles of the latter.

The maximum drift range $\Delta\theta_{max}$ imposed by each protocol when CPD = 0.5 rad is illustrated in

Figure 13c. Most of the one-sided loading histories exhibit a smaller $\Delta\theta_{max}$ compared to the conventional *SAC protocol*. More specifically, the *OD-1* ($\theta_{init} = 0.01, 0.02$), *OD-2* ($\theta_{init} = 0.01, 0.02$), and *OD-3* ($\theta_{init} = 0.01, 0.02$) loading protocols are characterized by smaller drift ranges and larger N_t than the conventional *SAC protocol*, while the *OD-4* ($\theta_{init} = 0.01, 0.02$) history is characterized by a similar $\Delta\theta_{max}$ and N_t as the conventional *SAC protocol*. This is because the CPD is related to both the plastic drift range and N_t. For a small plastic drift range, a larger N_t is required to reach the targeted CPD. The target values of $\Delta\theta_{max}$ for the conventional *SAC protocol* were found to be 0.05 rad (i.e., earthquake having a 10% probability of exceedance in 50 years), and 0.08 rad under the ground motions of (i.e., earthquake having a 2% probability of exceedance in 50 years). These values are also plotted in Figure 13c (horizontal red lines).

3.4 Categorization of the one-sided loading histories

In this section the ability of the developed one-sided loading histories (Figure 10) to impose ductility demands similar to those recoded during the FE time-history analysis of steel MRFs (Section 2), is assessed. In Figure 14 the mean drift - CPD relationships as developed for each one-sided loading history (i.e., red and blue lines in Figure 14a and 14b, respectively) are compared to the mean drift - CPD relationships of critical columns as obtained from the frame analysis (i.e., grey lines in Figure 14a and 14b). This figure indicates that the developed one-sided loading histories successfully trace the whole range of the one-sided hysteretic behaviour of the frames. As shown in Figure 14a, the lower bound of the one-sided hysteretic behaviour can be fairly simulated by employing the *OD-1* and the *OD-2* ($\theta_{init} = 0.01$), while as shown in Figure 14b, the upper bound of the one-sided deformation histories can be fairly simulated by employing the *OD-3* and the *OD-4* ($\theta_{init} = 0.02$). Moreover, by observing Figure 14 it can be seen that the *OD-3* and *OD-4* ($\theta_{init} = 0.01$) loading histories produce similar results with the two collapse-consistent protocols shown in Figure 9. This clearly suggests that *OD-3* and *OD-4* alone may not be always realistic in simulating the one-sided hysteretic demands. It should be noted that the rainflow cycle counting method [9] was adopted to account only for the plastic loading cycles and the associated amplitudes per cycle in

the calculation of CPD related to the frame analyses. Krawinkler [9] reported that a primary consideration should be given to the cycles with relatively large deformation ranges, which will dictate damage accumulation. An additional consideration should be given to a conservative representation of the plastic deformation ranges.

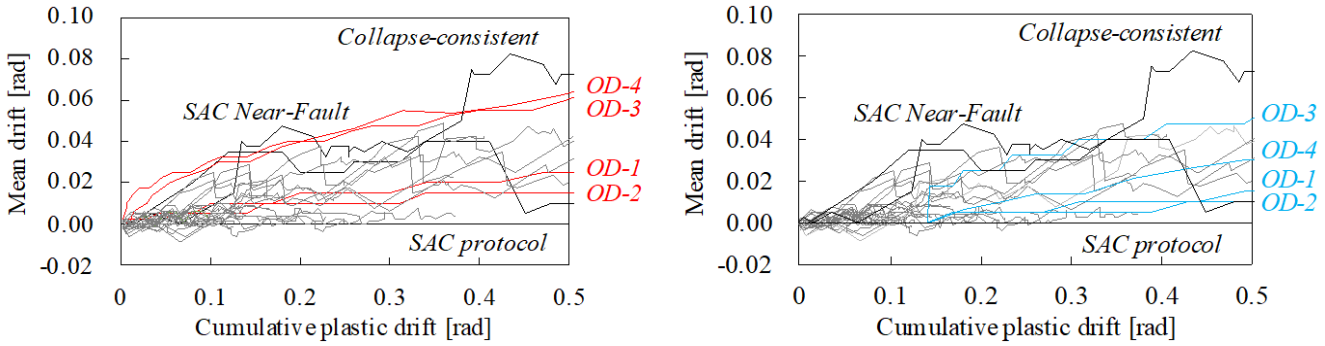

Figure 14 Comparison between the mean drift - CPD relationship for frame columns as obtained from the full-scale FE time-history analysis of steel MRFs and the mean drift - CPD relationship as obtained from the developed set of the one-sided loading histories for (a) θ_{init}= 0.01 rad, and (b) θ_{init}= 0.02 rad.

Notice: *grey lines refer to time-history analysis results of steel MRFs; red and blue lines to one-sided loading protocols; black solid lines to collapse-consistent protocols*

Finally, as it can be seen in Figure 13a, the *OD-1* ($\theta_{init} = 0.01$) imposes a similar number of cycles with the conventional *SAC protocol* when CPD = 0.5 rad. Accordingly, as shown in Figure 13b, the *OD-1* and the *OD-2* ($\theta_{init} = 0.01$) impose a similar maximum drift with the one suggested by the SAC program. The *OD-3* and the *OD-4* (θ_{init} = 0.01) loading histories varied from the target values, but the *OD-3* and *OD-4* loading histories with θ_{init} = 0.02 impose a relatively close drift to the target value. In Figure 13c, the *OD-2* ($\theta_{init} = 0.01$) reaches the smallest value for the maximum drift range while the *OD-4* ($\theta_{init} = 0.02$) the largest one. These findings in addition to the fact that these loading histories successfully simulated the one-sided hysteretic demands on frame columns as shown in Figure 14, including the upper and lower boundaries of the asymmetrical response, make them more suitable for assessing the hysteretic performance of components under one-sided cyclic loading. Therefore, among the developed set of one-sided loading histories introduced in Figure 10, the *OD-1* ($\theta_{init} = 0.01$), *OD-2* ($\theta_{init} = 0.01$), *OD-3*

($\theta_{init} = 0.02$), and *OD-4* ($\theta_{init} = 0.02$) are employed in the subsequent parametric study on the hysteretic behaviour of tubular steel columns.

4 One-sided hysteretic behaviour of steel tubular columns

An experimental investigation is performed in this section on the one-sided asymmetric cyclic behaviour of square tubular steel columns (SHS columns). On the basis of the test findings, numerical FE models are validated. Then, a numerical database of the predicted inelastic response of SHS columns made of both conventional and higher strength steels (involving high *Y/T* steels) is developed by subjecting column FE models of various *D/t* ratios to the previously identified one-sided cyclic loading histories. Emphasis is given on the evaluation of the inelastic behaviour of the more susceptible to local buckling high *Y*/*T* steel columns taking into consideration the lower hysteretic demands imposed by the one-sided cyclic loading. Based on the column response database, the current ductility and compactness classification limits for steel tubular columns are discussed in detail. The parametric study is conducted with the aid of an online computational platform that synchronizes MATLAB [42] and ABAQUS [26].

4.1 Experimental behaviour

Experiments are conducted to investigate the one-sided asymmetric cyclic behaviour of square tubular steel columns and are used for the validation of the column FE models. The test columns are two cantilevers subjected to symmetrical and asymmetrical cyclic horizontal loads, and constant axial compression [43]. The cyclic loading histories adopted herein for the test column 1 and test column 2 are shown in Figure 15a and Figure 15b, respectively. Figure 15c depicts the experimental set-up alongside with specimen dimensions. Both test columns are fabricated by a cold-formed SHS section made of the Japanese steel grade SN490B material (assumed equivalent to BCP325) and have a height of 780 mm, width of 200 mm and thickness of 9 mm. The actual width-to-thickness ratio is 21.9 and the corner curved region of the tube has a radius of 3.5 times the tube thickness. The vertical distance from the loading point to the column base is 1,015 mm. At the loading point, a constant axial load equal to 2,284 kN is applied, which corresponds to an axial load ratio of 0.25.

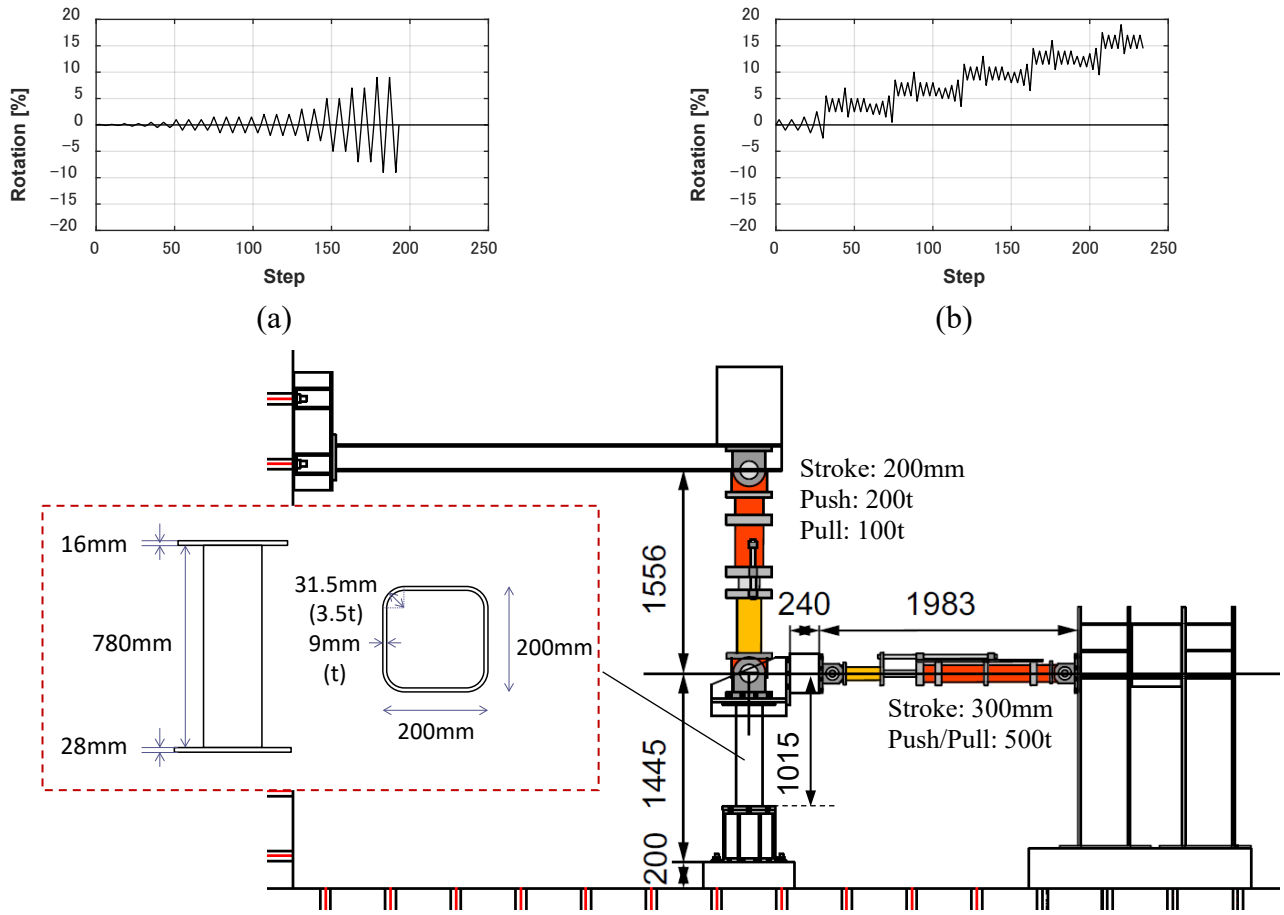

Figure 15 Cyclic loading histories of the column rotation (drift) and experimental set-up: (a) symmetrical SAC protocol, (b) one-sided asymmetrical cyclic loading history, and (c) dimensions of the test column specimens and overall view of the test set-up [43]

Figure 16a and Figure 16b depict the experimental moment – drift relationship of the column for the symmetrical and one-sided cyclic loading histories, respectively. By comparing these two flexural responses one can observe the less strength degradation and the more ductile response of the column under the one-sided loading history (test column 2). This is related to the delay of local buckling initiation and cyclic strain hardening behaviour of the material. Figure 16c shows the local buckling of the plastic hinge region as this has been developed after the completion of the symmetrical cyclic loading in test column 1. Accordingly, Figure 16d shows the plastic hinge region at 7% and 19% column rotation (drift), respectively, for the test column 2 which was subjected to the one-sided cyclic loading. The local buckling growth is found to be significantly less pronounced in test column 2 than that observed when the same column is subjected to a symmetrical cyclic loading protocol (i.e., SAC protocol). Local buckling initiated at 5% drift

for the test column 1, while during the second cycle of 7% drift the column lost approximately the 50% of its maximum flexural strength. On the contrary, a slight local buckling was observed in test column 2 at 8% drift which resulted in a more gradual strength reduction with the increase of the lateral drift. At 19% drift, test column 2 maintained nearly the 65% of its maximum flexural strength. Fracture was no observed in both specimens. It is worth noticing that the lateral loading history shown in Figure 15b was generated by repeating five times the cyclic loading history shown in Figure 9 (i.e., sequential loading). This ensured a similar reduction of the flexural strength of the columns under symmetrical and asymmetrical loading (Figs 16a and 16b), while local buckling is fully formed within the plastic hinge zone (Figure 16d).

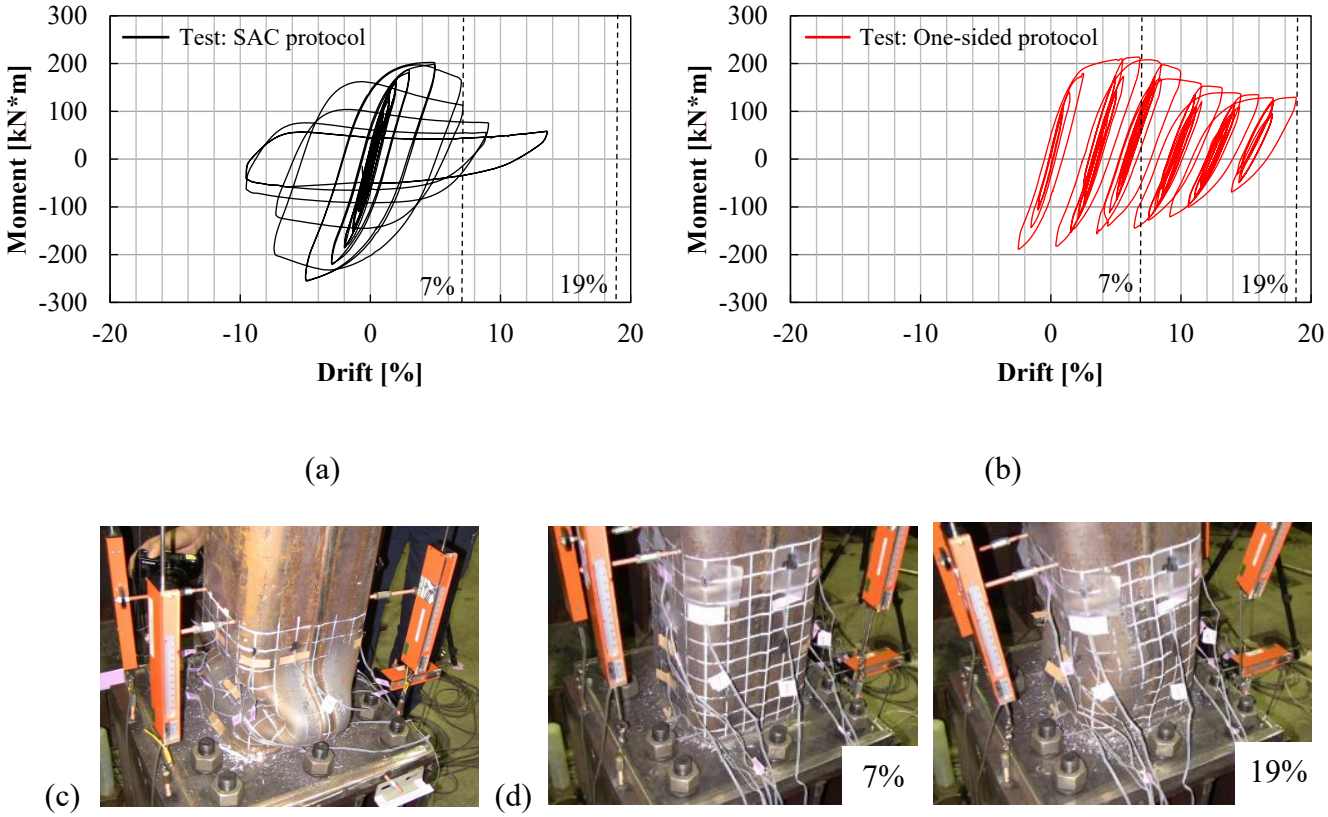

Figure 16 (a) Symmetrical moment – drift relationship of the test column 1; (b) one-sided asymmetrical moment – drift relationship of the test column 2; (c) picture of the plastic hinge region (local buckling) in test column 1 after the completion of the symmetrical loading history; and (d) picture of the plastic hinge region (local buckling growth) in test column 2 at the 7% and 19% column rotation (drift) of the one-sided cyclic loading history.

4.2 Development of the column FE model and experimental validation

A detailed FE model is developed and validated with the experimental results of columns. The column FE model is developed in ABAQUS [26] using S4R shell elements to discretise the entire member length. A finer mesh is assigned to the base of the column for a height equal to the column width to capture the growth of local buckling and the associated strength and stiffness deterioration, as shown in Figure 17a [25]. Figure 17b shows coupon tensile test results for the flat parts and the corner regions of the tested columns. The combined isotropic-kinematic hardening model available in ABAQUS material library which accounts for both the expansion and shift of the yield locus in stress space [44] is adopted herein to capture both the actual material strain-hardening and the effect of cyclic response. The backstress and the yield surface can be associated through material parameters calibrated automatically either from cyclic material test data or from the first half cycle of a unidirectional tensile coupon test (true stress and strain values). In this study, the half cycle data are used as obtained from coupon test results of the flat and corner region of the column (Figure 17a); this approach is usually adequate when the simulation involves low cycle loading histories [26]. The adopted material model in this section shall be considered accurate enough in simulating the strain hardening of steel and its effect on the one-sided ductility capacity of columns. On the contrary, the adoption of a more generalized hardening model in Section 2 (i.e., 1% of the modules of elasticity) was found to be a reasonable approach for introducing the required conservatism in the identification of the asymmetrical seismic demands at a frame level (i.e., one-sided loading histories).

Figure 17c compares the moment – drift relationship as obtained from the experimental results of test column 2 and FE analysis. A good agreement is observed between the two hysteretic responses. The strength deterioration due to local buckling initiation and the one-sided post-buckling response was successfully captured. A similar accuracy in simulations was observed for the test column 1.

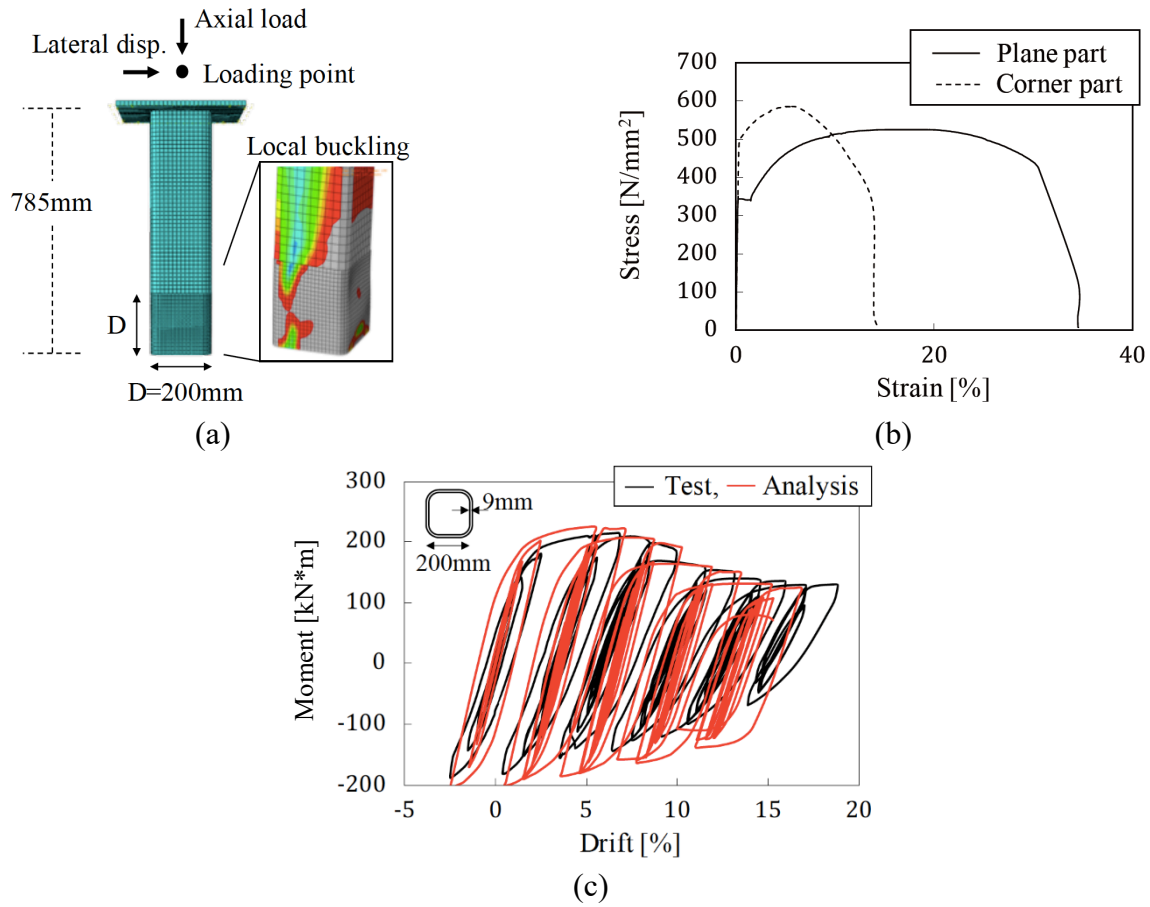

Figure 17 (a) Material properties of the steel SHS column made of SN490 grade steel plate (assumed equivalent to BCP325), (b) overview of the FE column model; and (c) comparison between test and FE analysis results on the moment – drift relationship of column test 2

4.3 Parametric study of columns

Based on the validated FE model described in the previous section, a parametric study is conducted to investigate the effect of key parameters such as steel grade and cross-section slenderness on the structural response of steel SHS. The effect of the loading history on the cyclic behaviour of the columns is assessed by subjecting them to the *conventional SAC* and the *SAC Near-Fault protocols*, as well as the *OD-1* ($\theta_{init} = 0.01$), *OD-2* ($\theta_{init} = 0.01$), *OD-3* ($\theta_{init} = 0.02$), and *OD-4* ($\theta_{init} = 0.02$) one-sided loading histories previously discussed. Six different material grades with varying *Y/T* ratios and four different *D/t* ratios of square tubular steel sections are considered, resulting in a total of 144 analyses.

4.2.1 Yield-to-tensile strength ratio (Y/T)

High strength steels provide relatively high *Y/T* ratio. The *Y/T* of structural steels is a measure of ductility of steel and greatly influences the inelastic behaviour and margins to plastic collapse of steel

sections. The various steels adopted in this study include conventional steels, steel with higher yield stress and steels with high *Y/T* ratio. The *Y/T* is considered as the primary characteristic of the material properties because it defines the level of hardening and the ductility capacity of the material [45]. High *Y/T* steels generally exhibit less ductility than conventional steels and are therefore not used in energy dissipative zones of earthquake resisting structures. The Canadian building design code limits the *Y/T* ratio up to 0.85 [1], while the American and European codes [5, 38] do not allow the use of steel grades with nominal yield stress more than 345MPa-380MPa (depends the structural system) for members in which inelastic behaviour is expected.

Table 5 lists the material properties of the Japanese steel grades investigated in this study, including high *Y/T* steels and high strength steels (i.e., yield stress higher than 345MPa). The nominal yield stress and the ultimate tensile stress as well as those obtained from tensile coupon tests (flat part and corner part of the tubes) are reported [46-48]. The corresponding stress-strain responses are illustrated in Figure 18. According to the specifications of structural steel materials available in the Japanese market the upper limit of *Y*/*T* ratio for conventional steels is considered 0.80. Thus, structural steels with a *Y*/*T* ratio higher than 0.80 are considered as high *Y/T* steels in this paper. The FE model discussed in Section 4.2 is adopted in this parametric study by employing the material test data reported in Table 5 and Figure 18.

Table 5 Steel materials used in parametric study of columns (flat and corner part of the steel tubes) [N/mm^2]

Steel materials	Flat Part			Corner Part		
	σ_y	σ_u	*Y/T*	σ_y	σ_u	*Y/T*
BCP235	285[a] (235[b])	476 (400)	0.60	442	511	0.86
BCP325	346 (325)	525 (490)	0.66	487	585	0.83
BCR295	338 (295)	460 (400)	0.74	468	551	0.85
UBCR365	443 (365)	539 (490)	0.82	610	635	0.96
BCHT385	465 (385)	634 (550)	0.73	575	667	0.86
BCHT400	441 (400)	527 (490)	0.84	534	585	0.92

[a] test values; [b] nominal values
Conventional steels: BCP235, BCP325, BCR295
Higher strength steels and steels with high *Y/T* ratio: UBCR365, BCHT385, BCHT400

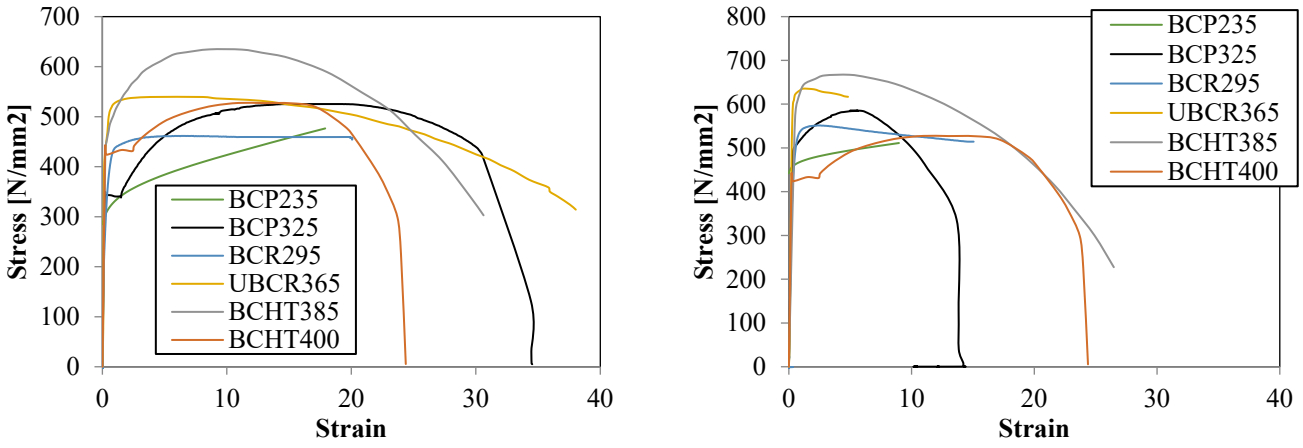

Figure 18 Stress-strain relationship for various conventional and high *Y/T* steels consider in this study: (a) flat part of the steel tubes; and (b) corner part of the steel tubes

497

498 ***4.2.2 Width-to-thickness ratio (D/t)***

499 The local buckling response of steel cross-sections subjected to compression, bending or
500 interactions thereof, is greatly affected by *D/t* of its constituent plate elements. It is noted in [49] that *D/t*
501 mainly determines whether a tubular column section can reach its plastic moment resistance prior to the
502 occurrence local buckling. In the Japanese design code, there are four discrete behavioural classes for cross-
503 sections called FA, FB, FC, and FD, corresponding to plastic/Class 1, compact/Class 2, semi-compact/Class
504 3 and slender/Class 4 sections in European design terminology. Cross-sections are assigned to one of these
505 classes based on the comparison of the width-to-thickness ratio of their most slender element against
506 codified slenderness limits. The procedure is conceptually identical to the cross-section classification
507 procedure specified in European [30] and American [5] design standards with the exception that there is no
508 distinction between plastic and compact sections in Ref. [31], i.e., all sections reaching their plastic moment
509 resistance are assumed to possess adequate rotation capacity. Table 6 shows the *D/t* limits for internal
510 elements in compression for each section class specified in the Japanese, American and European structural
511 steel design codes. For completeness, the revised more stringent slenderness limits specified in Ref. [32],
512 which will replace Ref. [30] are also included. In all design standards the slenderness limits depend on the
513 yield stress F_y of the element being classified. Table 7 reports the class of the four cross-sections employed

for the column for each of the six steel materials adopted in the parametric study according to the Japanese design standards [49]. Brackets are used for combinations of material and section geometries currently not available in the market, which are however included in this study for research purposes.

Table 6 Width-to-thickness ratio limits for internal elements in compression according to international design standards

Design standard	Plastic / FA	Compact / FB	Semi-compact / FC
AIJ [47]	$33\sqrt{235/F_y}$	$37\sqrt{235/F_y}$	$48\sqrt{235/F_y}$
EN 1993-1-1: 2014[28]	$33\sqrt{235/F_y}$	$38\sqrt{235/F_y}$	$42\sqrt{235/F_y}$
prEN 1993-1-1: 2019 [30]	$28\sqrt{235/F_y}$	$34\sqrt{235/F_y}$	$38\sqrt{235/F_y}$
AISC: 2016 [29]	-	$32.67\sqrt{235/F_y}$	$40.84\sqrt{235/F_y}$

Table 7 Class of column cross-sections considered in the parametric study according to AIJ [46]

D/t	BCP235	BCP325	BCR295	UBCR365	BCHT380	BCHT400
31 (□-500/16)	FA	FB	FB	FC	(FC)	(FC)
26 (□-500/19)	FA	FA	FA	FA	FA	FB
23 (□-500/22)	FA	FA	FA	FA	FA	FA
20 (□-500/25)	FA	FA	FA	(FA)	FA	FA

4.4 Performance indices

To facilitate the discussion on the obtained results and quantify the effects of the investigated parameters on the ductility capacity of the simulated columns, two performance indices are defined, namely the plastic rotation ratio, μ (or ductility), and the cumulative plastic rotation ratio, η (or cumulative ductility). The ductility and the cumulative ductility indices are obtained from the envelope curve and the cyclic response, respectively, and are defined in the following equations:

$$\mu = \theta_{M_{max,85\%}}/\theta_y \tag{4}$$

$$\eta = \Sigma\theta_p/\theta_y \tag{5}$$

where $\theta_{M_{max,85\%}}$ is defined as the rotation at which the envelope curve of the hysteresis cycles falls below 85% of the maximum value after the peak strength is reached, θ_y is the yield rotation defined as the rotation corresponding to 0.2% plastic rotation and $\Sigma\theta_p$ is the cumulative plastic rotation corresponding to the attainment of $\theta_{M_{max,85\%}}$. According to Newell and Uang (2006) [50] who investigated the cyclic behaviour of steel columns under symmetrical loading histories, a 10% reduction from M_{max} was suggested to define the rotation capacity. In this study, considering that one-sided loading histories strongly affect local buckling growth in columns (see Figure 16), a 15% reduction (i.e., 85% of the maximum strength) was adopted to ensure that the local buckling has been fully developed within the plastic zone.

4.5 Analysis results

Figure 19 illustrates representative results of the parametric study under the one-sided loading histories. Corresponding results of columns subjected to conventional and near-fault protocols are shown for comparison. The monotonic lateral loading curves (pushover curves) for each column case are plotted in red colour. The maximum flexural strength (M_{max}) and the 85% of the maximum flexural strength ($M_{max,85\%}$) are marked on the envelop curves. Strength deterioration is caused by local buckling. Fracture is not simulated in the present study. By comparing the one-sided hysteretic response to the pushover curves, the level of strength deterioration imposed by each loading history can be assessed and discussed. The *OD-1* and *OD -2* loading histories impose severe strength deterioration while the *OD-3* and *OD-4* lead to responses closer to the pushover curves. Hence, protocols *OD-1* and *OD -2* are deemed able to define the lower bound of the capacity of the one-sided inelastic response, while the *OD-3* and *OD-4* protocols are able to define the upper bound of the capacity of the one-sided inelastic response, as conceptually introduced in Figure 1.

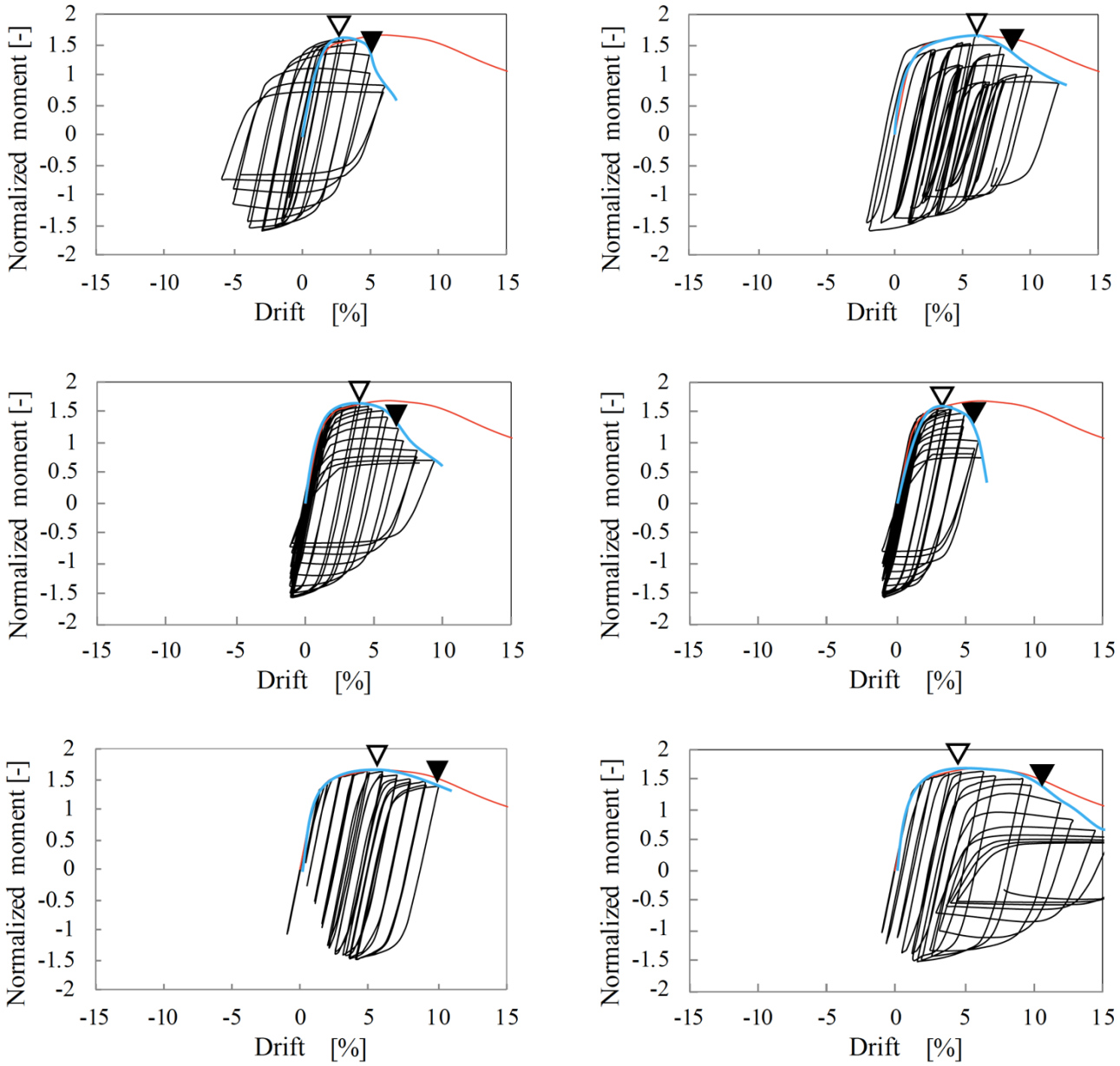

Figure 19 Column responses to the symmetrical and one-sided cyclic loading (BCP325, *D/t*=20): (a) Conventional SAC protocol, (b) SAC Near-Fault protocol, (c) *OD-1* ($\theta_{imit} = 0.01$), (d) *OD-2* ($\theta_{init} = 0.01$), (e) *OD-3* ($\theta_{init} = 0.02$), and (f) *OD-4* ($\theta_{init} = 0.02$)

Figure 20 shows the impact of the asymmetry in loading history on the ductility demands for columns. The ductility μ, as defined in Eq. (4), is plotted against the *D/t* for columns made of BCP325 (conventional steel) and BCHT400 (high *Y/T* steel) under the conventional *SAC protocol* and the developed one-sided loading histories. The black curves refer to conventional steel column and the red curves refer to high *Y/T* steel column. The solid lines refer to the response under the conventional *SAC protocol* while the

dashed lines refer to the average response under the four identified one-sided loading histories (*OD-1*, *OD-2*, *OD-3* and *OD-4*). The columns with plastic and compact class cross-sections exhibited around a 10% reduction in ductility when the high *Y/T* steel was used in place of the conventional steel under the symmetrical cyclic loading, whereas the columns under the one-sided cyclic loading exhibited a 20% to 70% increase in the attained ductility. Thus, the asymmetry in loading history has a strong influence on the ductility capacity of columns, while as expected, strain hardening appears to have an influence on the ductility capacity of columns demonstrating the rationality of this study to explicitly account for the actual stress-strain relationship in strain hardening model of columns (Section 4.1). Therefore, a new normilized index is introduced herein that accounts for both the *D/t* and *Y/T* as shown in Eq. (6). By using this normalized index, the influence of the loading histories on the various steel grades can be investigated in detail.

$$D/t \cdot (Y/T)/0.8 \tag{6}$$

where 0.8 indicates the limit of high *Y/T* ratio steels according to Japanese construction.

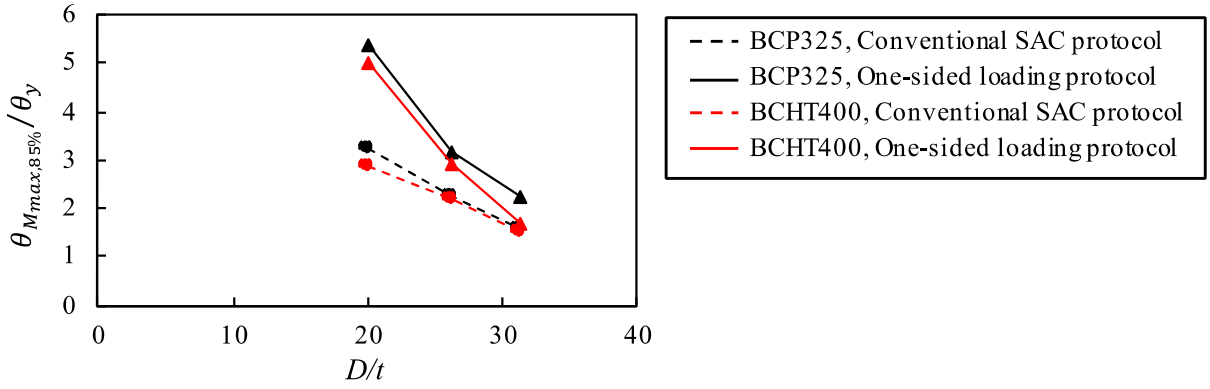

Figure 20 Relationship between *D/t* ratio and plastic ratio $\mu = \theta_{M_{max,85\%}}/\theta_y$ for BCP325 and BCHT400 columns under the conventional SAC and the one-sided cyclic loading histories

Figure 21 presents the relationship between the normalized *D/t* and the ductility, μ. In addition to the newly suggeted normalization of *D/t* introduced by Eq. (6), the normalization index $D/t \cdot \sqrt{\sigma_y/E}$ that is commonly used in design codes [37, 49] is illustrated. The new normalization index shows a stronger

correlation between the *D/t* and μ (Figure 21b). As reference results, in this figure results obtained from the pushover loading and the conventional *SAC protocol* are plotted along with their regression curves (red and black colour, respectively). The columns under pushover loading showed the highest ductility capacity since the absence of loading cycles eliminated the damage accumulation and the corresponding ductility reduction present in all cyclic loading protocols. The columns under one-sided loading histories exhibited a higher ductility than those under the conventional *SAC protocol*. Table 8 lists the ratio of the average one-sided ductility to the conventional ductility; it ranged from 1.15 to 1.71. Results confirmed the previous finding that the *OD-2* ($\theta_{init} = 0.01$) and the *OD-3* ($\theta_{init} = 0.02$) loading histories define a lower and upper bound of the inelastic capacity, respectively, with respect to ductility. For the lower bound values, the cumulation of damage through many repeated drift ranges that include cyclic reversals of negative yield drifts ($-\theta_{init}$) (see Figure 10b) resulted in higher ductility demands. On the contrary, the relatively high values of maximum drifts and drift ranges combined with many loading cycles with no cyclic reversals of $-\theta_{init}$ (see Figure 10c) defined the upper capacity bound. It should be noted that these bounds are crossed at the range of normalized *D/t* higher than 1.2 for normalization $D/t \cdot \sqrt{\sigma_y/E}$, and higher than 25 for normalization $D/t \cdot (Y/T)/0.8$ (Figure 21). As a result, the previously defined lower and upper bounds are reversed for this range of *D/T* ratios. This change in tendency is related to the characteristics of the one-sided loading protocols. Thin steel sections or sections made of higher *Y/T* ratios were found to be more susceptible to local buckling under the *OD-3* than the *OD-2* because of the existence of higher maximum drifts in the *OD-3* (see Figure 10c).

The evaluation of the column capacity under the one-sided loading history may allow the use of higher *D*/*t* ratios reaching a similar ductility to the one determined by the symmetrical loading history. This can allow the use of higher strength steels, such as the high *Y/T* steels or steel with high yield stress, in column areas prone to non-linearity. It appears that high *Y/T* steel columns with FA class cross-section exhibit an increased margin to local buckling initiation and a sufficient ductility afterwards. This study aimed to quantify the favoured one-sided ductility capacity when limited by local buckling failures. Whether this holds true for other failure modes (e.g., fracture) is a subject of future work.

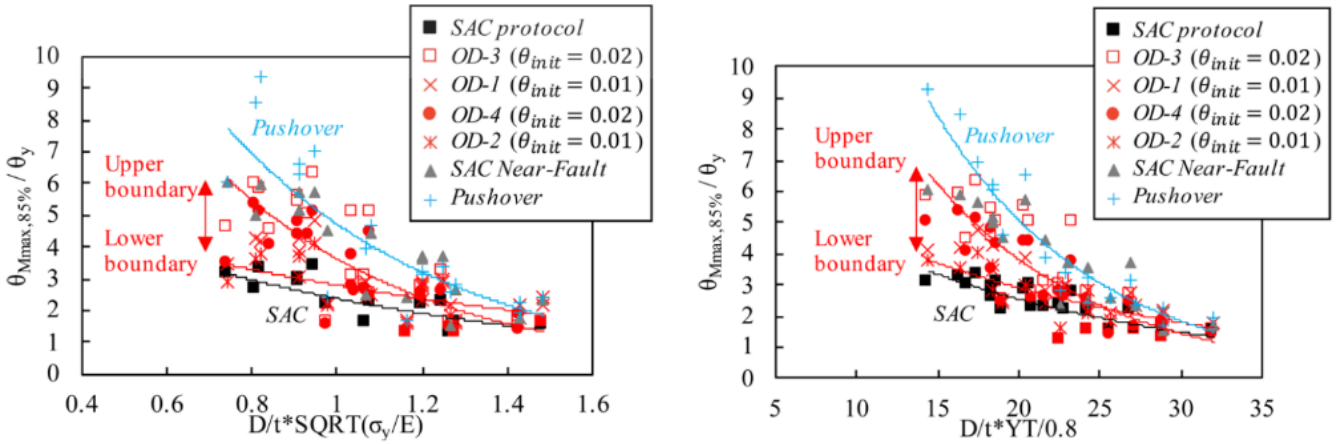

(a) (b)

Figure 21 Ductility ratios, μ against: (a) $D/t \cdot \sqrt{\sigma_y/E}$; and (b) $D/t \cdot (Y/T)/0.8$

600

Table 8 Average values of μ and η as determined from the results of the one-sided cyclic loading histories in relation to the results under the conventional loading protocol

Ratio (one-sided history / SAC protocol)	***SAC* / *SAC***	*OD-3* / *SAC*	*SAC N.F.* / *SAC*	*OD-1* / *SAC*	*OD-4* / *SAC*	*OD-2* / *SAC*
$\mu = \theta_{M_{max,85\%}}/\theta_y$	**1.00**	1.15	1.31	1.67	1.71	1.71
$\eta = \Sigma\theta_p/\theta_y$	**1.00**	1.20	1.21	1.22	1.41	1.41

601

602 Figure 22 illustrates the relationship between the maximum drift and the CPD for each loading
603 protocol considered in this study. This figure describes the growth of one-sided deformation as controlled
604 by the loading protocols in terms of maximum drift. The curve for the *OD-2* ($\theta_{init} = 0.01$) is almost
605 identical with that of conventional *SAC protocol*. This is in accordance with the finding for the upper and
606 lower bound mentioned above. Thus, the curves shown in Figure 22 closer to the right indicate lower
607 ductility demands corresponding to the upper capacity bound of the one-sided inelastic response (*OD-3*),
608 while the curves closer to the left indicate higher ductility demands corresponding to the lower capacity
609 bound of the one-sided inelastic response (*OD-2*).

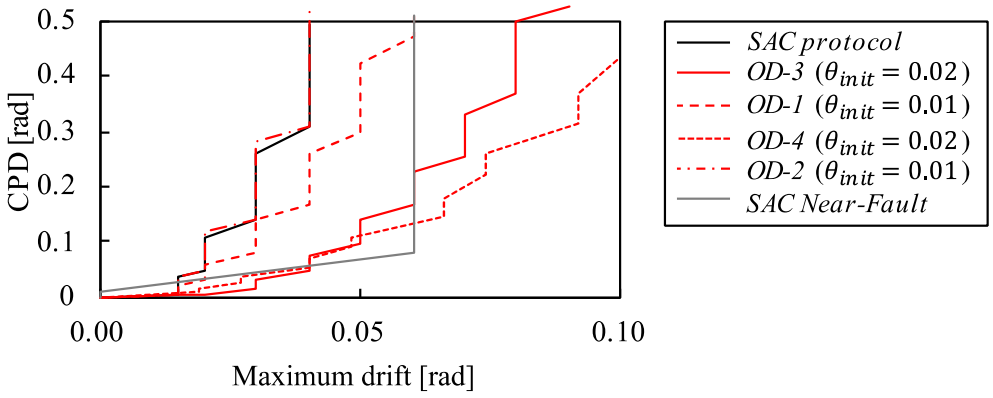

Figure 22 Evolution of one-sided deformation in terms of maximum drift

Finally, Figure 23 plots the relationship between the normalized *D/t* and the cumulative ductility, η, as defined in Eq. (5). As reference results, in this figure results obtained from the conventional *SAC protocol* are presented. The columns subjected to symmetrical cyclic loading exhibited the lowest η for each value of $D/t \cdot YR/0.8$. The columns under the one-sided loading protocols exhibited higher η than those under the conventional *SAC protocol*. It is noted that when $D/t \cdot YR/0.8 < 21$ (Plastic / FA sections only), η strongly depends on the type of loading protocol, while it seems there is no significant influence for normalized values of *D/t* higher than 21. Table 8 lists the ratio of the average one-sided cumulative ductility to the conventional cumulative ductility; it ranged from 1.20 to 1.41.

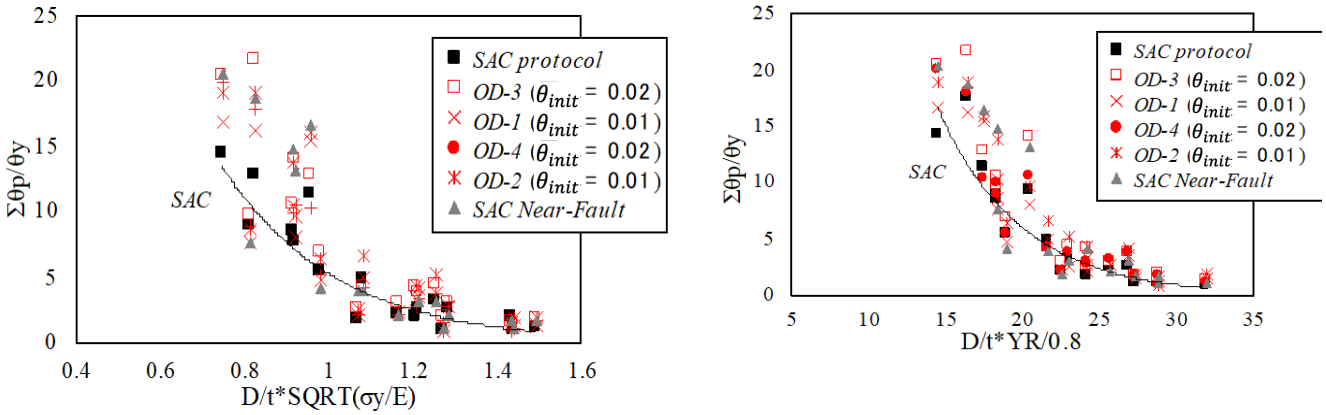

(a) (b)

Figure 23 Cumulative ductility ratios, η against: (a) $D/t \cdot \sqrt{\sigma_y/E}$; and (b) $D/t \cdot (Y/T)/0.8$

5 Seismic behaviour of frames with high *Y/T* steel columns

In this section, the seismic performance of a newly designed five-story five-bay steel MRF with

tubular steel columns made of conventional steel (BCR295) and high *Y/T* steel (BCHT400) is investigated. Full-scale FE nonlinear static (pushover) and dynamic time-history analyses under two hazard levels. The two hazard levels considered are named as Level 1 and Level 2 earthquakes, respectively, defined by the design spectrum and the associated maximum ground velocity (PGV), which in turn gives approximate return periods. The Level 1 corresponds to PGV of 25 cm/sec and return period of 50 years, while the Level 2 correspond to PGV of 50 cm/sec and return period of 500 years, approximately [52, 53]. Table 9 shows the design characteristics of the conventional steel MRF (Original frame) and the high *Y/T* steel MRF (Alternative frame). Using the same ductility demands for the columns of the original frame, a new normalized *D*/*t* can be defined from Figure 21 for the column sections of the alternative frame. The normalized *D*/*t* can increase from 20.9 to 24.2 in order to retain a similar strength capacity (M_p) having a reduced section area (*A*). Accordingly, the bending stiffness (*EI*) is reduced. The high *Y/T* steel columns are classified as plastic/FA sections, while the limit for the normalized *D/t* ratio for Class 1/FA is equal to 25.3 for BCHT400 steel (F_y=400 N/mm^2).

Table 9. Design characteristics and properties of the conventional steel MRF and high *Y*/*T* steel MRFs

	Original frame (Conventional MRF)	Alternative frame (High *Y/T* MRF)
Height [mm]	20,500	
Span [mm]	6,400	
Story height [mm]	3,950	
Natural period [sec]	0.94	1.06
Column material	BCR295	BCHT400
Beam material	SN490B	SN490B
Column section at all stories	SHS-500×22	SHS-450×19
Column *D/t* (Class)	22.7 (FA)	23.7 (FA)
Column $D/t \cdot YT/0.8$	20.9	24.2
Column M_p $[kN \cdot m]$	1,991 (100%)	1,858 (93%)
Column EI $[kN \cdot m^2]$	307,500 (100%)	190,010 (62%)
Column Area [cm^2]	404 (100%)	309 (76%)
Beam sections at 1st and 2nd story	H-600×250×12×22	
Beam sections at 3rd, 4th and 5th story	H-600×250×12×19	
Floor gravity loads external / internal columns [kN]	198.4 / 396.8	
Top floor gravity loads external / internal columns [kN]	235.2 / 470.4	

Figure 24 compares the pushover curves of both frames (i.e., base shear coefficient vs. roof drift). The alternative frame reaches a similar maximum strength (lower by 7%) and exhibits a larger resistance to the initiation of the post-yielding behaviour than the original frame (10 % higher). For comparison, the

initiation of the post-yielding behaviour in this figure was determined when the plastic roof drift exceeded 1/500 rad. Both the original and alternative frames did not experience any sudden strength deterioration. For seismic forces having a higher probability of occurrence than the design seismic action (i.e., frequent events checked for a base shear coefficient of 0.2), the roof drift in the original and alternative frame was found to be 1/320 rad and 1/260 rad, respectively. Both values satisfy the Japanese Building Standard regulations [51] which limit the drifts to 1/200 rad. This drift limitation is similar with the "damage limitation requirement" in European standards [38]. It appears that the lower flexural stiffness provided by the high *Y/T* steel MRF is adequate to restrain the lateral deformation at this performance level despite the reduction in the cross-section area of the column nearly at 25%.

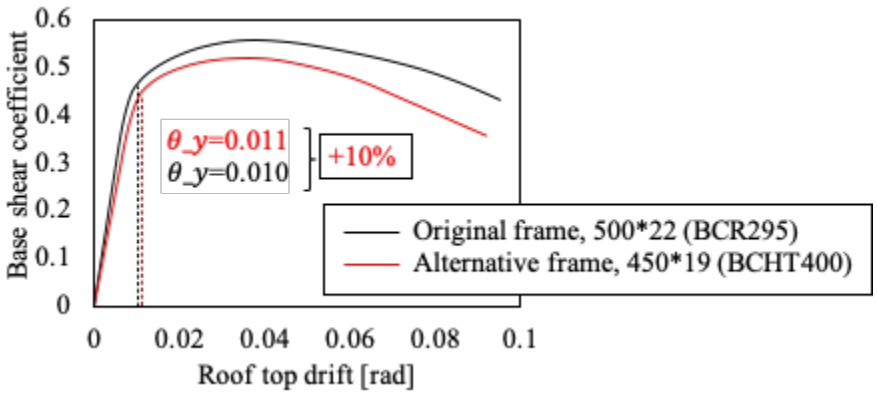

Figure 24 Comparison of the pushover curves between the original and alternative steel MRFs

Three pulse type ground motions, the *JMA_Kobe,* the *Taft,* and the *Miyagioki*, are selected and scaled to the Level 1 (PGV: 25 cm/s) and Level 2 (PGV: 50 cm/s) hazard levels. The purpose of Level 1 evaluation is to ensure that a building remains within the elastic range. At Level 2 evaluation, a building is intended to be repairable even if it reaches the plasticity range when subjected to an earthquake whose return period is approximately 500 years [52, 53]. The considered story ductility (maximum drift over yield drift) for Level 2 ground motions should be less than 2. Figure 25 shows the acceleration spectra of the selected ground motions. The natural periods of both the original and alternative frame design are 0.94 and 1.06 sec, respectively. Figures 26 and Figure 27 show the relationship between the story drift and the base shear coefficient and the drift time history of the first-story columns for the Level 1 and Level 2 ground

656 motions, respectively.

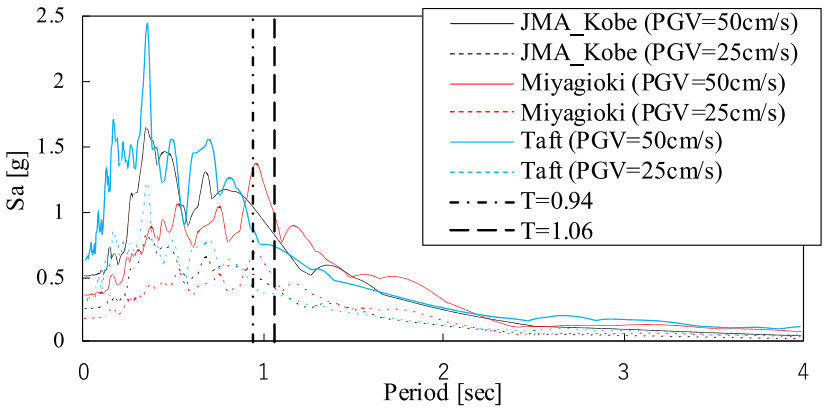

Figure 25 Acceleration spectra of the selected ground motions and natural periods of the steel frame models

657
658

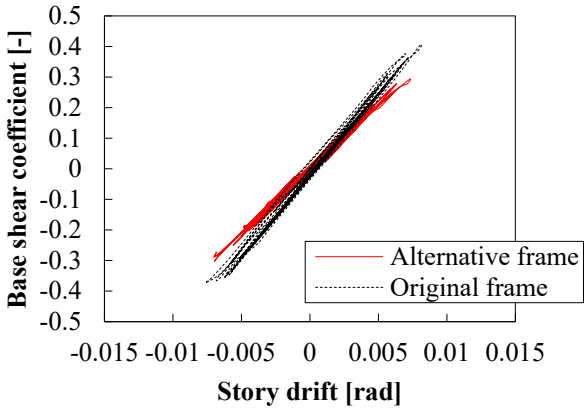

(a)-1

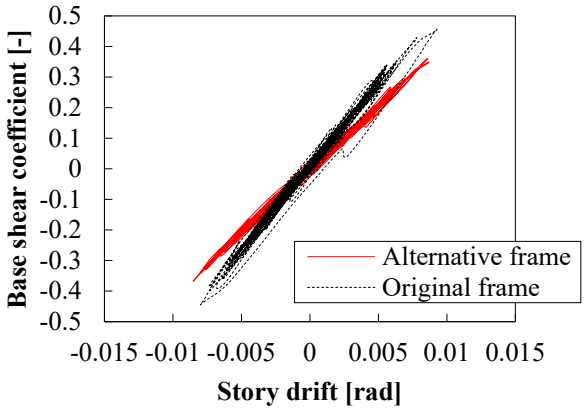

(a)-2

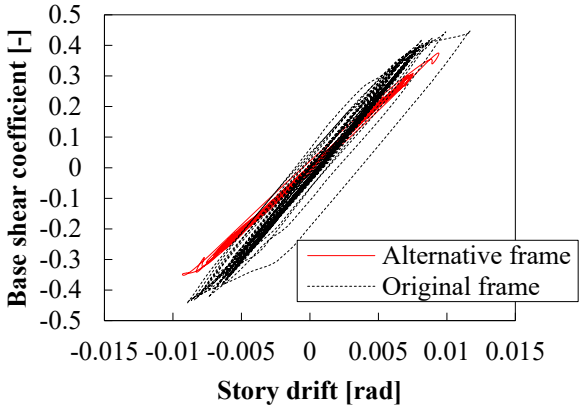

(a)-3

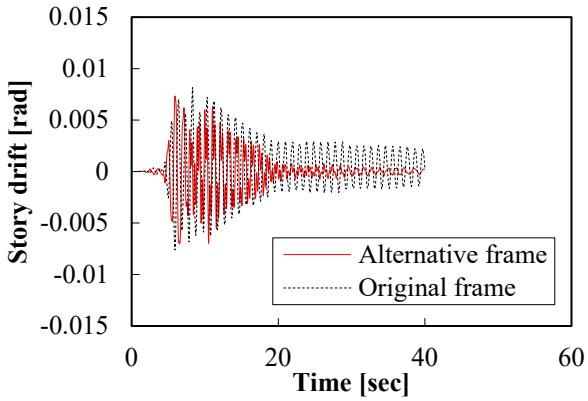

(b)-1

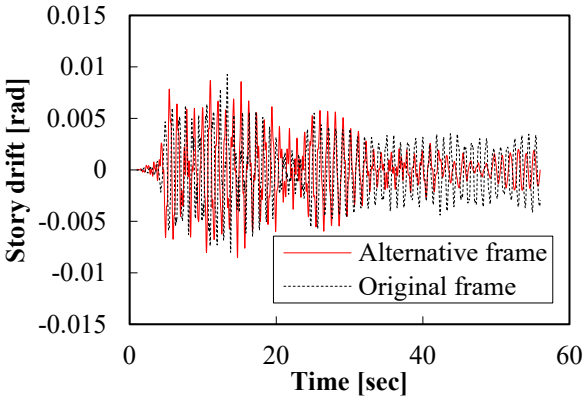

(b)-2

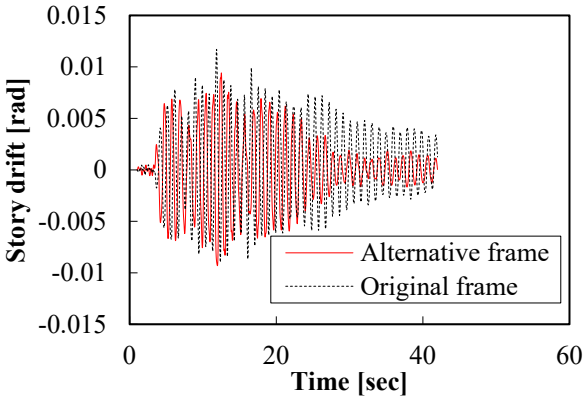

(b)-3

Figure 26 Comparison of the seismic response of the original and alternative steel MRF against Level 1 ground motions; (a) hysteretic loop in terms of base shear coefficient and maximum story drift, (b) drift time-history of the 1st story (1: J*MA_Kobe*, 2: *Taft*, 3: *Miyagioki*)

659

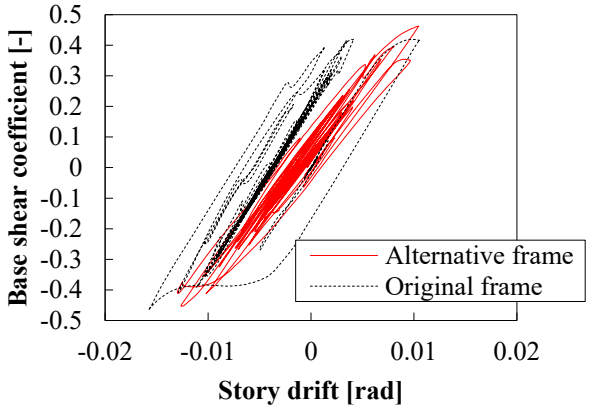

(a)-1

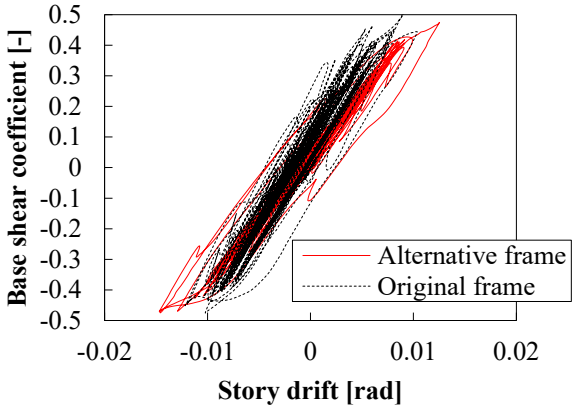

(a)-2

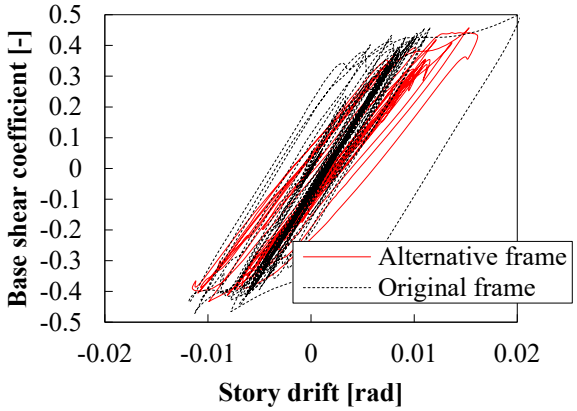

(a)-3

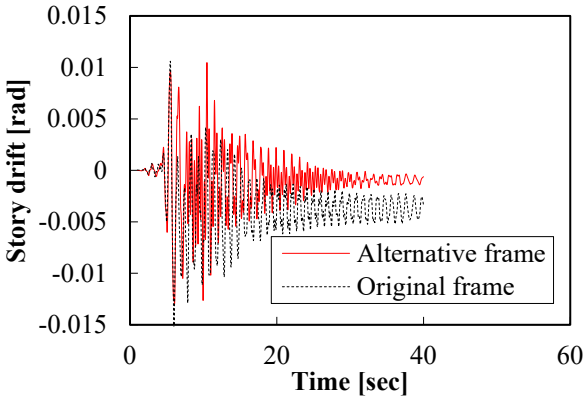

(b)-1

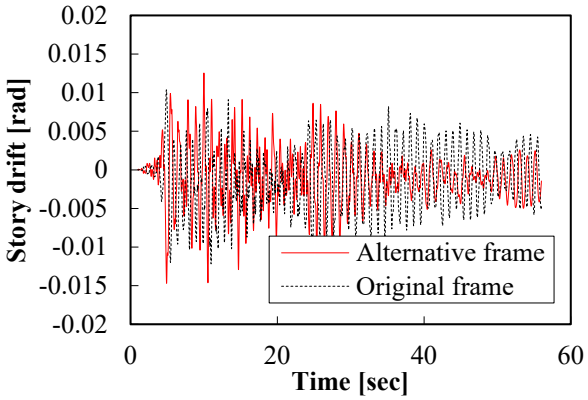

(b)-2

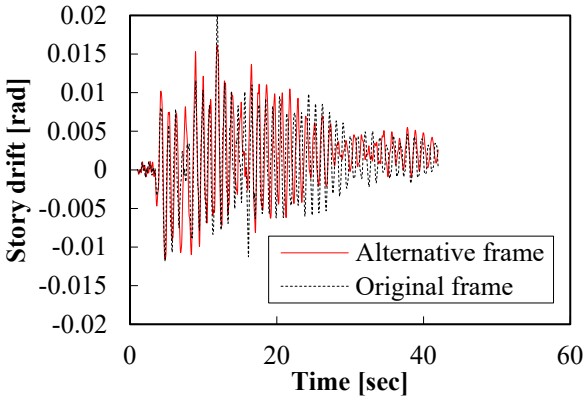

(b)-3

Figure 27 Comparison of the seismic response of the original and alternative steel MRF against Level 2 ground motions; (a) hysteretic loop in terms of base shear coefficient and maximum story drift, (b) drift time-history of the 1st story (1: J*MA_Kobe*, 2: *Taft*, 3: *Miyagioki*)

660

Table 10 Seismic responses of the original and alternative steel MRF in terms of yield story drift, maximum story drift, story ductility and residual story drifts against each ground motion and hazard intensity level

PGV	EQ	Original MRF				Alternative MRF			
		Yielding drift (θ_y)	Maximum drift (θ_{max})	Story Ductility	Residual drift (θ_{res})	Yielding drift (θ_y)	Maximum drift (θ_{max})	Story Ductility	Residual drift (θ_{res})
(25cm/s)	*JMA_Kobe*	0.0063	0.0082	1.37	-	-	0.0073	<1.00	-
	Taft	0.0063	0.0092	1.44	-	0.0083	0.0087	1.05	-
	Miyagioki	0.0063	0.0120	1.88	-	0.0083	0.0094	1.13	-
(50cm/s)	*JMA_Kobe*	0.0063	0.0158	2.63	0.0037	0.0083	0.0130	1.57	0.0009
	Taft	0.0063	0.0122	1.91	0.0008	0.0083	0.0147	1.77	0.0007
	Miyagioki	0.0063	0.0204	3.19	0.0019	0.0083	0.0162	1.96	0.0026

661

662 Table 10 lists the yield drifts, the maximum story drifts and the story ductility, as well as the residual
663 roof story drifts after each earthquake motion and hazard intensity level. As it can be seen in Figure 26, the
664 alternative frame design has a 30% lower elastic stiffness than the original frame and remained almost
665 elastic under the Level 1 ground motions. The original frame under the same ground motions yielded and
666 reached an average story ductility and an average maximum drift equal to 1.56 (max: 1.88) and 1.00%
667 (max: 1.20%), respectively (Table 10). Figure 27 shows that the columns in both frames were plastified
668 under the Level 2 ground motions. The alternative frame reached an average story ductility and an average

maximum drift equal to 1.77 (max: 1.96) and 1.46% (max: 1.62%), respectively. The original frame reached an average story ductility and an average maximum drift equal to 2.57 (max: 3.19) and 1.61% (max: 2.04%), respectively. For all the cases, the moment attains to 1.1 of M_p, thereby a similar strength capacity is provided by the alternative frame design. It appears that the more susceptible to local buckling high Y/T steel columns can resist the earthquake loads without exhibiting any strength deterioration (i.e., local buckling).

Overall, under the Level 1 ground motions, the alternative frame exhibited approximately a 10% smaller story drift than that of the original frame. Under the Level 2 ground motions, the alternative frame yielded at a 1.25 to 1.38 times higher story drift than the original frame, while the experienced maximum and residual drifts of the alternative frame appeared to be in some cases 20% and 75% lower than those in the original design, respectively (Table 10). Therefore, under the same strength requirements for both steel MRFs, the more flexible design of the high Y/T steel MRF naturally affects the seismic performance of the frame resulting in a later yielding and smaller story drift ductility demands. This behaviour combined with the increased margins to local buckling initiation due to the one-sided hysteretic behaviour may lay the basis for a new design framework that allows the use of higher strength steels on regions of a structure prone to nonlinearity. Further studies are required to generalize the findings of the present work.

6 Conclusions

This study investigated the local buckling behaviour of tubular steel columns made of high yield-to-tensile strength ratio (Y/T) steels subject to one-sided cyclic loading. The one-sided loading histories were first developed on the basis of a seismic response databank on the asymmetrical hysteretic behaviour of various steel moment-resisting frames (MRF). This study experimentally proved the favoured one-sided cyclic ductility capacity of columns as limited by local buckling, and then computationally suggested that high Y/T steel columns may have an increased capacity margin to local buckling initiation and a sufficient ductility afterwards (i.e., ductility bonus). Thus, high strength steels may be suitable for energy dissipative members resulting in reduced material consumption and more economical seismic design of steel structures.

695 The main conclusions are as follows:

696 (1) Based on the seismic responses of the frames under consideration, the one-sided behaviour depends
697 on the column-to-beam moment ratio at frame joints. The asymmetry of the one-sided hysteretic
698 behaviour of the frames increases as the moment ratio decreases. The frame with the lower moment
699 ratio (=1.2) suffered from the whipping effect. The level of residual deformations and the direction
700 of response is primarily affected by the ground motion, and secondly, by the level of axial load.

701 (2) Eight types of one-sided loading histories were developed, but four were identified as suitable to
702 simulate the one-sided asymmetrical hysteretic demands as derived from the gradual progress of local
703 buckling. These loading histories successfully traced the cumulative damage that was developed in
704 the columns during the frame time-history analyses and can define an upper and lower bound for the
705 corresponding one-sided ductility for a wide cross-section slenderness range.

706 (3) The local buckling growth was found to be significantly less pronounced in the asymmetrically loaded
707 test column than that observed when the same column was subjected to a symmetrical cyclic loading.
708 Local buckling initiated at 5% drift for the symmetrically loaded test column, while during the second
709 cycle of 7% drift the column lost approximately the 50% of its maximum flexural strength. On the
710 contrary, a slight local buckling was observed in the asymmetrically loaded test column at 8% drift.
711 At 19% drift, the test column maintained nearly the 65% of its maximum flexural strength.

712 (4) For evaluating the ductility performance of square tubular steel columns with various Y/T, a new
713 normalization of the width-to-thickness ratio (D/t) was suggested by using the factor $D/t \cdot$
714 $(Y/T)/0.8$. This new normalization index reflects the effect of the Y/T ratio improving the overall
715 distribution of the results. Based on this new index the one-sided ductility capacity of columns and
716 ductility bonus can be better assessed, and new section classification limits can be explored with
717 clarity.

718 (5) To evaluate the effectiveness of each one-sided loading history, the number of cycles, the maximum
719 drift, and the maximum drift range were examined. High values of maximum drifts combined with

small maximum drift ranges define a low-ductility demand history driven by large residual deformations (upper bound). On the contrary, a larger number of repeated cycles in conjunction with smaller peak drifts but large drift range appear to form a high-ductility demand history (lower bound). The upper and lower bound scenarios are reversed for high normalized *D/T* ratios.

(6) The one-sided ductility capacity ratios of the steel columns were found to be on average 1.15 (lower bound) to 1.71 (upper bound) times the corresponding ratios identified under the symmetrical conventional protocol. A higher reserve capacity was observed for the columns employing a plastic/FA section. Similarly, the one-sided cumulative ductility ratios were found to be on average 1.20 to 1.41 times higher than those defined under the conventional protocol. In terms of ductility, this capacity enhancement was clearly observed for the entire range of values of the normalized *D*/*t* ratio. In terms of cumulative ductility, a minor difference between the one-sided and conventional response was observed for normalized *D*/*t* higher than 21.

(7) Based on the identified column ductility capacities, two five-story five-bay steel MRFs were designed with plastic/FA columns made of conventional and high *Y/T* steels, respectively. While both frames provided a similar lateral strength, the high *Y/T* steel MRF enjoyed nearly 25% smaller column cross-sectional area. Under the more likely to occur earthquakes, the high *Y/T* steel MRF behaved elastically, while the ground floor columns of the conventional steel MRF yielded at the base. Under rare seismic events the more susceptible to local buckling high *Y*/*T* steel columns resisted the earthquake loads without exhibiting any strength deterioration. The average story drift ductility demand for the high *Y/T* steel MRF was less than the threshold of 2.00 (i.e., 1.77), while that for the conventional steel MRF was 2.57.

(8) The proposed design of steel MRFs using higher strength steels with relatively high *Y*/*T* ratio resulted in later column yielding and smaller story drift ductility demands than the conventional design. This behaviour combined with the increased resistance of steel tubular columns to local buckling due to the favoured one-sided hysteretic behaviour of steel MRFs, may lay the basis for the development of a seismic-resilient design framework where critical members can remain elastic under frequent

earthquake events and exhibit low damage under rare events. This would overcome current limitation in using higher strength steels that inherently provide a high *Y/T* on regions of a structure prone to nonlinearity.

Acknowledgement

The authors are grateful to Dr Yosiki Ikeda, Professor of Kyoto University, for his valuable comments and encouragement throughout this project. The first author is thankful to the University of Birmingham, UK, for hosting him as a Visiting Research Student. The authors are also grateful to Dr Yusuke Suzuki from Nippon Steel Corporation for his valuable comments and the provision of material data.

References

1. Sivakumaran KS. Role of yield-to-tensile strength ratio in the design of steel structures. In: Jansto SG, Patel J, editors. Niobium Bearing Structural Steels, The Minerals, Metals & Materials Society; 2010, p. 63–76.
2. SAC Joint Venture. Protocol for fabrication, inspection, testing, and documentation of beam-column connection tests and other specimens. SAC/BD-97/02 Version 1.1, October. Sacramento, CA: SAC: 1997.
3. European Convention for Constructional Steelwork (ECCS). Recommended testing procedure for assessing the behaviour of structural steel elements under cyclic loads. Report N^{o} 45. 1st Edition. Brussels: ECCS; 1986.
4. Applied Technology Council (ATC). Guidelines for cyclic seismic testing of components of steel structures. ATC-24. Redwood City, CA: ATC; 1992.
5. American Institute of Steel Construction (AISC). Seismic provisions for structural steel buildings. ANSI/AISC Standard 341-16. Chicago: AISC; 2016.
6. Federal Emergency Management Agency (FEMA). Interim protocols for determining seismic performance characteristics of structural and nonstructural components through laboratory testing.

Technical Report FEMA 461. Washington, DC: FEMA; 2007.

7. Vian, D, Bruneau M. Tests to structural collapse of single degree of freedom frames subjected to earthquake excitations. Journal of Structural Engineering – ASCE 2003; 129(12): 1676-1685.

8. Eggers D, Baig MMI. Significance of ratcheting in seismic analyses: In Proceeding of Structural Mechanics in Rector Technology (SMiRT-23), August 10-14, 2015, Manchester, United Kingdom. Paper No. 358

9. Federal Emergency Management Agency (FEMA). Effects of strength and stiffness degradation on seismic response. Technical Report FEMA P-440A. Washington, DC: FEMA; 2009.

10. Ghassemieh M, Rahimzadeh A. Impact of loading protocol on the performance of the steel moment frame connections. Journal of Rehabilitation in Civil Engineering 2018; 6-2: 115-138.

11. Krawinkler H, Gupta A, Medina R, Luco N. Development of loading histories for testing of steel beam-to-column assemblies. Stanford. CA. 2000; 94305-4020.

12. Krawinkler H. Loading Histories for cyclic tests in support of performance assessment of structural components. 3rd International Conference on Advances in Experimental Seismic Engineering, PEER. 2009.

13. Kato A, Fukuda J, Nakagawa S, Obara K. Foreshock migration preceding the 2016 Mw 7.0 Kumamoto earthquake, Japan. Geophysical Research Letters 2016; 43: 8945–8953. doi:10.1002/2016GL070079.

14. Faisal A, Majid TA, Hatzigeorgiou GD. Investigation of story ductility demands of inelastic concrete frames subjected to repeated earthquakes. Soil Dynamics and Earthquake Engineering 2013; 44: 42-53.

15. Moustafa A, Takewaki I. Response of nonlinear single-degree-of-freedom structures to random acceleration sequences. Engineering Structures 2011; 33: 1251-1258.

16. Ke K, Chen Y. Seismic performance of MRFs with high strength steel main frames and EDBs. Journal of Constructional Steel Research 2016; 126: 214-228.

17. Zhai CH, Wen WP, Li S, Xie LL. The influences of seismic sequence on the inelastic SDOF systems:

In Proceedings of 15th WCEE World Conference on Earthquake Engineering, Lisbon, Portugal, 2012.

18. Takemura H, Kawashima K. Effect of loading hysteresis on ductility capacity of reinforced concrete bridge piers. Journal of Structural Engineering 1997; 43A: 849-858. https://www.researchgate.net/publication/285025641
19. Hatzivassiliou M, Hatzigeorgiou GD. Seismic sequence effects on three-dimensional reinforced concrete buildings. Soil Dynamics and Earthquake Engineering 2015; 72: 77-88.
20. Paul WR, Uang C-M. Testing protocol for short links in eccentrically braced frames. Journal of Structural Engineering 2006; 132(8):1183-1191.
21. Al-Janabi M, Topkaya C. Nonsymmetrical loading protocols for shear Links in eccentrically braced frames. Earthquake Engineering and Structural Dynamics 2020; 49: 74-94.
22. Suzuki Y, Lignos DG. Development of collapse-consistent loading protocols for experimental testing of steel columns. Earthquake Engineering and Structural Dynamics 2020; 49: 114-131.
23. Mergos PE, Beyer K. Loading protocols for European regions of low to moderate seismicity. Bulletin of Earthquake Engineering 2014; 12: 2507-2530.
24. Maison BF, Speicher MS. Loading Protocols for ASCE 41 Backbone Curves. Earthquake Spectra 2016; 32(4): 2513-2532.
25. Skalomenos KA, Hatzigeorgiou GD, Beskos DE. Parameter identification of three hysteretic models for the simulation of the response of CFT columns to cyclic loading. Engineering Structures 2014; 61: 44–60.
26. Dassault Systems, Simulia Corp. ABAQUS version 2016 documentation, Providence: Dessault Systems,Simulia Corp.; 2016.
27. Architectural Institute of Japan (AIJ). Ultimate strength and deformation capacity of buildings in seismic design. Tokyo: AIJ; 1990.
28. Architectural Institute of Japan (AIJ). Recommendation for limit state design of steel structures. Tokyo: AIJ; 2010.

821 29. Structural technical standard manual for buildings. Tokyo: ICBA; 2020.
822 https://kenbokyo.jp/book/item.html?bid=80
823 30. European Committee for Standardisation (CEN). EN 1993-1-1:2005+A1:2014. Eurocode 3. Design of
824 steel structures. General rules and rules for buildings. Brussels: CEN; 2014.
825 31. American Institute of Steel Construction (AISC). Specification for structural steel buildings.
826 ANSI/AISC Standard 360-16. Chicago: AISC; 2016
827 32. European Committee for Standardisation (CEN). prEN 1993-1-1:2019. Eurocode 3. Design of steel
828 structures - Part 1-1: General rules and rules for buildings. CEN/TC 250. Brussels: CEN; 2019.
829 33. BlueBEAR. High-performing computer (HPC) at the University of Birmingham,
830 http://www.bear.bham.ac.uk/bluebear/
831 34. The Building Center of Japan (BCJ). National Research and Development Corporation Architectural
832 Research Institute. 2005Ver. design and construction manual for cold-formed tubular column. Tokyo:
833 BCJ; 2005.
834 35. Skalomenos KA, Papazafeiropoulos G. A computational method for performing nonlinear adaptive
835 pushover analysis of structures through ABAQUS simulation: In Proceedings of 7th COMPDYN
836 International Conference on Computational Methods in Structural Dynamics and Earthquake
837 Engineering, Heraklion, Crete, Greece. 2019. https://doi.org/10.7712/120119.7199.19194
838 36. Gardner L, Wang F, Liew A. Influence of strain hardening on the behaviour and design of steel
839 structures, International Journal of Structural Stability and Dynamics 2011, 11(5): 855-875
840 37. European Committee for Standardisation (CEN). EN 1993-1-5. Eurocode 3: Design of steel structures
841 – Part 1-5: Plated structural elements. Brussels: CEN; 2006.
842 38. European Committee for Standardisation (CEN). EN 1998-1 (2004). Eurocode 8. Design of structures
843 for earthquake resistance, Part 1: General rules, seismic actions and rules for buildings. Brussels: CEN;
844 2004.
845 39. Pacific Earthquake Engineering Research (PEER) Center. PEER strong motion database.

(http:www.peer.berkeley.edu/smcat)

40. Zhai CH, Wen WP, Li S, Xie LL. The influence of seismic sequence on the inelastic SDOF systems. Proceedings of 15WCEE, Lisbon, Portugal, 2012.

41. Hasegawa T. Shaking table test on earthquake response behaviour of 2-story frames composed of H-shaped steel beam and column with yielding joint panel zone. Journal of Structural and Construction Engineering 2004; 69(578): 139-146.

42. MATLAB. The language of technical computing, Version 2018a. The Math- works Inc.: Natick, Mass., USA, 2018.

43. Inada K, Sasaki S, Skalomenos KA, Kurata M. Experimental investigation of hollow structural section columns subjected to asymmetric loading protocols, Part II: Test Results. In Proceedings of the Annual Meeting of the Architectural Institute of Japan, AIJ, 4 - 6 September 2018, Tohoku University, Sendai, Japan. Paper No. 22585

44. Smith, M. ABAQUS/Standard User's Manual, Version 6.14. Dassault Systèmes Simulia Corp, Providence, RI, 2009.

45. Bannister AC, Trail SJ. Structural integrity assessment procedures for European industry. British steel 1996.

46. Nakagawa H, Sato Y, Okada T. Structural performance of cold-roll-forming hollow section using 490N/mm^2 steel, Part1: Bending Test. In Proceedings of the Annual Meeting of the Architectural Institute of Japan, AIJ, 13 September 2014, Kobe University, Hyogo, Japan. Paper No. 22483

47. Arita M, Yamaguchi T, Sawaizumi S, Suzuki Y, Suzuki T, Maeda S. Structural performance of cold press formed rectangular column using 550N/mm^2 high strength steel, Part 1: Mechanical properties and performance of welded joints. In Proceedings of the Annual Meeting of the Architectural Institute of Japan, AIJ, 23 August 2011, Waseda University, Tokyo, Japan. Paper No. 22341

48. Kubota S, Yamaguchi T, Suzuki Y, Suzuki T. Structural performance of cold press formed rectangular column using high yield strength steel, Part1: Mechanical properties and performance of plates and welded Joints. In Proceedings of the Annual Meeting of the Architectural Institute of Japan, AIJ,

872 10 September 2010, Toyama University, Toyama, Japan. Paper No. 22458

873 49. Architectural Institute of Japan (AIJ). Recommendations for stability design of steel structures. Tokyo:
874 AIJ; 2009

875 50. Newell J, Uang C-M. Cyclic behavior of steel columns with combined high axial load and drift demand,
876 Report No. SSRP-06/22, The University of California, San Diego, 2006

877 51. The Building Center of Japan (BCJ). The Building Standard Law of Japan: Tokyo: BCJ; 2016.
878 https://www.bcj.or.jp/publication/detail/17/

879 52. Japan Structural Consultants Association (JSCA). Draft of JSCA Performance-based Design Manual
880 for Seismic Performance. Tokyo: JSCA; 2016.

881 53. Otsuki Y, Buyco K, Kurata M, Speicher M. Feasibility study on multi-code seismic evaluation of a
882 landmark building: In Proceedings of 11th NCEE U.S. National Conference on Earthquake Engineering,
883 Los Angeles, California. June 25-29, 2018.